RECOMPILATION OF LITHOLOGICAL PROXIES ACROSS THE
PERMIAN-TRIASSIC BOUNDARY

by

HEATHER NICOLE BRAUER

Presented to the Faculty of the Graduate School of

The University of Texas at Arlington in Partial Fulfillment

of the Requirements

for the Degree of

MASTER OF SCIENCE IN GEOSCIENCE

THE UNIVERSITY OF TEXAS AT ARLINGTON

December 2020

Acknowledgements

Abstract

RECOMPILATION OF LITHOLOGICAL PROXIES ACROSS THE

PERMIAN-TRIASSIC BOUNDARY

Heather Brauer, MS

The University of Texas at Arlington, 2020

Supervising Professor: Arne M. E. Winguth

The largest mass extinction occurred near the Permian-Triassic boundary (PTB; 251.902 ± 0.024 Ma; Shen et al., 2011), with the demise of more than 90% of marine species and 70% of terrestrial species. This study expands sedimentary data bases created by Rees and others (2002) and the PALEOMAP Project by Scotese (2001). Lithological data was categorized as Upper Permian (259.1-254.902 Ma) or Lower Triassic (251.902-247.2 Ma), and the paleogeographic information of the proxies were reconstructed using GPlates 2.0. These lithological proxies are compared with climate sensitivity simulations from the fully coupled comprehensive Community Climate System Model (CCSM3). The climate simulation using radiative forcing 4 x CO_2 relative to preindustrial atmospheric levels (or 4 x CO_2 PAL) is consistent the reconstruction of Late

Permian whereas the most extreme scenario, climate conditions of a 12.7 x CO_2 simulation with lower cloud optical depth may be comparable to the hothouse climate of the Early Triassic as inferred from the sedimentary record.

Table of Contents

List of Figures

Chapter 1

Introduction

1.1 The end-Permian extinction

Understanding rapid climate transitions of the past is of importance to improve prediction of climate change in the future. One of the largest and most rapid climate transitions in the geologic history occurred from the Paleozoic to Mesozoic eras (Rees et al., 2002) across the Permian-Triassic boundary (PTB; 252.28 ±0.08 Ma; Shen et al., 2011). This transition into a hothouse world (Joachimiski et al., 2012, Sun et al., 2012), is characterized by the most severe mass extinction in the Phanerozoic. This wide scale biotic catastrophe is referred to as "The Great Dying" as a result of the extinction of more than 90% of marine species (Raup, 1979; Erwin, 1993), and 70% of terrestrial species (Maxwell, 1992; King, 1991). The recovery of marine and terrestrial species was a protracted process that exceeded 5 million years (Twitchett, 1999; Payne et al., 2006; Bottjer et al., 2008). The end-Permian extinction can give context to understanding the scale and rate of the current mass extinction of species under anthropogenic-induced climate change.

1.2 The Permian-Triassic boundary

The formal designation of the Permian-Triassic boundary is the Global Stratotype Section and Point (GSSP) recognized in the base of Bed 27c of the Meishan Section D, Changxing County, Zhejiang Province South China based on the first occurrence of the conodont *Hindeodus parvus* (Yin et al., 2001). *Hindeodus parvus* has been discovered in shallow water and pelagic deposits (Kozur, 1996; Lai, 1998; Yin et al., 2001) and is an exceptional index marker because it is not latitudinally restricted; however, using a marine organism such as *H. parvus*, does not assist in establishing terrestrial boundaries.

Problems may arise when using the occurrence of *H. parvus* to correlate sections because this conodont may have appeared earlier or later in global sections other than in Meishan. According to Ellwood et al. (2017), the Lowest Observed Occurrence Point (LOOP) should be used in identifying the lowest appearance of *H. parvus* in sections other than at the GSSP section. Correlation to a GSSP is difficult and not always based on the local first occurrence of the boundary identifying taxa; therefore, graphic correlation (Shaw, 1964; Edwards, 1984, 1989) or constrained optimization (Kemple et al., 1995; Sadler, 2004), should be used in identifying the Permian-Triassic boundary in sections other than the GSSP section. Notably, graphic correlation to Meishan has been successful, utilizing

9

magnetic susceptibility, stable isotope and elemental chemistry, and biostratigraphic analyses, in the marine sections of Lung Cam, Vietnam (Nestell et al., 2015), and Slovenia (Lan et al., 2018). The same types of taxa found in the free specimens of foraminifers and microconchids in the Lung Cam section, can been seen from other Permian-Triassic sections in Iran (Brönnimann et al., 1972); Hungary (Bérczi-Makk, 1987); Italy (Groves et al., 2007); Turkey (Groves et al., 2005).

Geochronological constraints surrounding the Permian-Triassic in most continental basins are poor; however, the Sydney-Gunnedah-Bowen Basin system in eastern Australia preserves a well-calibrated and complete stratigraphic record (Fielding et al., 2019). The Permian-Triassic boundary was equated with the first common occurrence of *Lunatisporites pellucidus* at the top of the Illawarra Coal Measures (Helby, 1973; Metcalfe et al., 2015). There is a consensus that the end of coal accumulation in the eastern Australian basins (Michaelsen, 2002; Metcalfe et al., 2015; Laurie et al., 2016) signifies a major crisis in terrestrial ecosystems (Fielding et al., 2019).

1.3 Causes of the end-Permian extinction

Several hypotheses have been proposed that suggest a synergistic effect of various mechanisms that caused the end-Permian extinction. One controversial proposal is that an extraterrestrial impact (Becker et al., 2001;

10

Kaiho et al., 2001; Basu et al., 2003) could have triggered rapid volcanism that produced the Siberian Traps (Renne and Basu, 1991; Renne et al., 1995; Kamo et al., 2003; Korte et al., 2010); however, extensive Siberian volcanism (Bowring et al., 1998), associated volatile releases (Black et al., 2012), and methane release by magmatic intrusion into coal beds (Svensen et al., 2009) are generally accepted as the main causes that triggered the extinction event (Fig. 1.1). Svensen et al. (2004) estimated approximately 100,000 Gt of carbon released by degassing of the Siberian Traps. There are uncertainties regarding the magnitude and timing of the carbon influx into the atmosphere and if it was a gradual, one-step, or a multi-stepped process (Payne and Clapham, 2012); however, associated greenhouse gas emissions derived from Siberian volcanism are presumed to have triggered a global climate change (Hallam and Wignall, 1997; Kidder and Worsley, 2004; Algeo et al., 2011; Retallack et al., 2011; Joachimiski et al., 2012) during the Late Permian to Early Triassic.
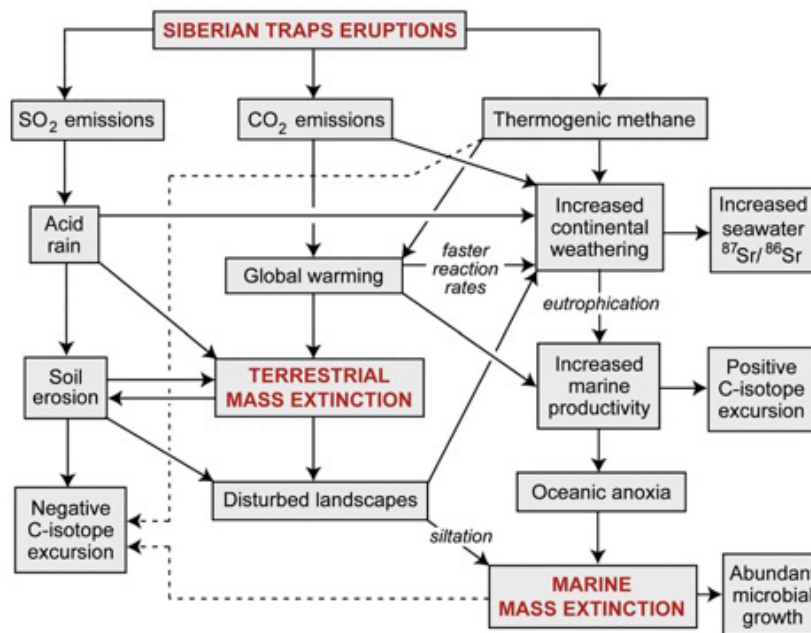
Figure 1.1 Flowchart model of cause-and-effect relationships during the end-Permian extinction. Modified from Wignall (2001) and Algeo et al. (2011).

The increased greenhouse radiative forcing from this event could have led to a climatic warming and increase in tropical sea surface temperatures (SSTs) that were detrimental to marine biota. In South China, $\delta^{18}O_{apatite}$ values from conodonts reveal a rapid increase in sea surface temperatures from 21°C to 36°C (over ~0.8 million years; Myr) that potentially exceeded 40°C by the Early Triassic (Sun et al., 2012). Furthermore, volcanic degassing could have led to enhanced production of carbon dioxide (Hallam and Wignall, 1997; Brand et al., 2012), and a change in ocean chemistry to acidic conditions (Payne et al., 2010), with a

change in ocean salinity (Kidder and Worsley, 2004). Acid rain (Benton and Newell, 2014), and wildfires (Algeo et al., 2011; Hudspith et al., 2014) devastated plants and the land which added nutrient input that stimulated the marine carbon pump. An enhanced carbon pump, ocean stratification, and global warming would have triggered widespread anoxia (Wignall and Twitchett, 1996; Isozaki, 1997) providing inhospitable conditions for marine biota.

Another factor that potentially exacerbated the extinction event was the size and configuration of the land and ocean during this time. Present-day Earth is uniquely divided by north-south trending continents and oceans that define climate biomes based on flora and fauna; however, by the Late Permian, most of the world's landmasses were amalgamated to form a supercontinent, Pangea (Köppen and Wegener, 1924), spanning from the northern landmasses Laurasia and southern continent Gondwana (Fig. 2.; Ziegler et al., 1997), which provided a wide expanse of tropical and subtropical land with minimum marine influence (Gordon et al., 1975). In addition, the Late Paleozoic superocean, Panthalassa, covered nearly two-
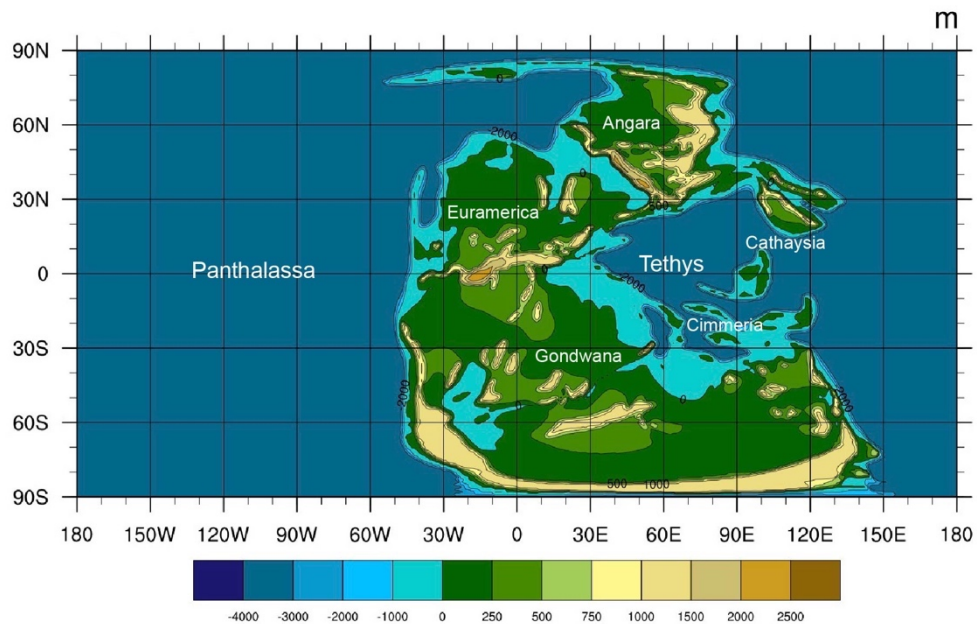
Figure 1.2 Reconstruction of the latest Permian paleogeography and topography from PALEOMAP Project by Scotese (2001).

thirds of the Earth's surface (Scotese, 1987) with a mediterranean sea, Tethys, that was partially enclosed by the Cimmerian microcontinents. The role of land and ocean distribution in shaping ancient climates has long been recognized and the differences in latent heat flux and heat capacity between land and ocean, would have greatly influenced atmospheric and oceanic processes that further exacerbated the extinction event. With one large landmass, we expect a maximum continentality and monsoon

14

circulations (Kutzbach and Gallimore, 1989). According to Ziegler (1982), Pangea showed signs of instability in the Late Permian and more so during the Triassic.

The geologic record contains globally lithological proxies that can be utilized to reconstruct past climate regions. The present study analyzes the paleogeographic distribution of lithological proxies across Pangea in conjunction with climate simulations to identify climate transitions across the Permian-Triassic boundary associated with the mass extinction event.

Chapter 2

Objectives

This study focuses on climate changes and the related paleogeographic distribution of lithological proxies in response to the perturbation in radiative forcing across the PTB. Lithological proxies as described by Ziegler et al. (1998) have been compared to simulations of a fully coupled climate-model (Winguth et al., 2015), similar to Gibbs et al. (2002) and Osen (2014), to understand the transition of climate regions during the onset and continuation of Siberian Flood volcanism. The comparison of these proxies with modeling studies could reveal large-scale change in the climate comparable to those we predict for the future (Kidder and Worsley, 2012). Understanding the Earth's historical response to greenhouse gas emissions could serve as a suitable analog for understanding the implications of anthropogenic induced climate change. The objectives for this study are the following:

1. Recompile a Late Permian to Early Triassic database of lithological proxies from Rees et al. (2002), the PALEOMAP Project by Scotese (2001).

2. Isolate controlling factors for each proxy formation and identify global distribution patterns of the lithological proxies across the Permian-Triassic boundary.

3. Compare the paleogeographic distribution of lithological proxies to simulated climate regions from a fully coupled comprehensive model (Community Climate System Model version 3.0; CCSM3).

Chapter 3

Lithological proxies

We begin our approach with present-day sedimentary rock formation and distribution. The present-day continental configurations and corresponding rock records have parallels to understanding past climate. Today, just as in the past, these rock types are influenced by biogeochemical and climatic changes. The later will be the focus of this study: patterns of lithological proxies will be compared with those inferred from paleoclimate simulations (e.g., Rees et al., 2002; Ziegler et al., 1998, 2003). Previous studies incorporate the following lithological proxies that may be suitable to infer past climatic conditions: peat and coal, evaporites (including, gypsum, halite and anhydrite), carbonate deposits and reefs. We analyze the global distribution of these proxies and apply present-day correlations of depositional settings with simulated climate conditions to reconstruct the climate zones of the past.

It must be noted that previous studies refer to the lithological proxies presented here as "climate-sensitive sediments"; although in geologic terminology, the term "sediment" is not equivocal to a rock. Moreover, although the present and previous studies utilize lithological proxies to infer climates of past, it must be emphasized that the formation of each sedimentary rock type is not restricted to a singularly defined depositional

environment; however, we will attempt to identify global trends and distribution patterns. A description of lithological proxies used in the present study and by Ziegler et al. (1998) is described in the following sections.

The formation of peat and coal occurs in regions characterized by wet or temperate climates that favor an excess of precipitation (Parrish et al., 1982; Hallam, 1985). Coal can form along equatorial regions near the intertropical convergence zone (ITCZ) where precipitation is continuous throughout the annual cycle. Other important rain-producing systems include the orographic and diurnal land-sea systems (Gyllenhaal et al., 1991) that can influence the formation of peat and coal as seen in upland peat deposits on mountainsides in deserts as a result of regular orographic precipitation. Peat also forms in mangrove swamps, which derive moisture from the seawater, not rainfall; however, mangrove peats are well developed in areas with the highest precipitation (Woodroffe et al., 1992).

Evaporites are minerals that are formed as precipitates from the evaporation of a saline solution. This study encompasses evaporitic salts such as, halite, gypsum, and anhydrite. These salt deposits form in environments with where evaporation exceeds precipitation and/or rate of water flow (Sellwood et al., 1993). Thick evaporite deposits are mostly formed behind a barrier beach or barrier islands with multiple inlets rather than in a basin within regions where a level of isolation from the ocean is

established. Today, these areas are limited to lagoons, but in the past evaporite basins reached millions of square kilometers (Ziegler et al., 1997). Evaporites typically form in arid regions associated with Earth's deserts which can form by various causes including, the descending limbs of the Hadley cell, continentality, and orography (Ziegler et al., 2003).

Carbonate formation is favorable in tropical and subtropical regions, approximately from 30° South to 30° North, that represent clear water associated with downwelling and low surface productivity. Transparent tropical water masses are dependent on light penetration which is a function of the solar zenith angle. Solar radiation with a high zenith angle on the sea surface has a low the albedo and thus a high amount radiation received at the sea floor in shallow subtropical waters (Ziegler et al., 1984) where most limestones are deposited. The subtropics are characterized by areas of Ekman convergence and high sea surface height that are typically centered over the high-pressure systems with low cloud cover, and thus low precipitation and low productivity thus enhancing the suitable clarity for reef formations. Chave (1967) pointed out that carbonates could form at all latitudes regardless of water temperature if the input of terrigenous clastic sediments was low. Modern limestones occur in the Caribbean Sea, Indian Ocean, Persian Gulf, Gulf of Mexico, around Pacific Ocean islands, and within the Indonesian archipelago. An example is the Bahamas Platform,

where abundant corals, algae and other organisms produce vast amounts of calcium carbonate skeletal debris that blanket the platform and producing extensive limestone deposit. A common misconception is that a warm water environment is essential for limestone formation because carbonate productivity is lowest in cold climates; however, the deposition of marine carbonate sediments in cool water environments has long been recognized (James, 1997) and some of the best exposed examples occur in Australia and New Zealand.

Present-day reefs are archetypal of tropical biomes because of the diversity of invertebrates, algae and fish. Sea surface height is crucial because photosynthesis supports the symbiotic zooxanthellae of reef-building corals. Coral formation favors oligotrophic waters with hospitable temperatures to sustain the symbiotic zooxanthellae that are critical for the survival of the coral reef. Because some carbonate and reef formation can be generally representative of warm tropical climate conditions influenced by oceanic processes, we focus on the factors that limit coral reef development including, temperature and light penetration to the sea floor. Reefs seem to be limited by temperature (Fraser and Currie, 1996) because warm temperatures enhance calcium carbonate precipitation. Using temperature as the only limiting factor for reef formation is controversial because some of the Earth's west-facing coasts are sufficiently warm, but

devoid of reefs (Vernon, 1995). Coral reefs are sessile organisms that are limited to latitudes where light refraction is continuous throughout the annual cycle and clastic runoff is minimal to not impede water clarity, particularly areas of Ekman convergence and associated high sea surface height. These factors are taken in consideration when comparing these lithological proxies with climate simulations (e.g. Gibbs et al., 2002; Winguth et al., 2002; Ziegler et al., 2003; Osen, 2014).

Chapter 4

Methodology

4.1 Community Climate System Model

A fully coupled comprehensive model, the Community Climate System Model version 3.0 (CCSM3), developed by NCAR has been applied for climate sensitivity experiments across the Permian-Triassic boundary.

The climate model CCSM3 consists of four components: the atmosphere, land, ocean and sea-ice (Collins et al., 2006a; Yeager et al., 2006; Kiehl and Shields, 2005) which are linked through a central coupler (CPL6). The model coupler exchanges the flux and state information among these components (Collins et al., 2006; Yeager et al., 2006; Kiehl and Shields, 2005). The model employs a spectral horizontal resolution of T31, which corresponds to a low resolution 3.75° × 3.75° grid and the vertical dimension consists of 26 unevenly spaced terrain-following levels (Collins et al., 2006). The Community Atmosphere Model version 3.0 (CAM3; Collins et al., 2004, 2006a) encompasses a zonal resolution of 3.75° at the equator for the T31 configuration. The Community Land Surface Model version 3.0 (CLM3; Oleson et al., 2004; Dickinson et al., 2006) utilizes the same horizontal grid as the atmosphere; however, each grid box is further divided into land units, soil columns, and plant types. CLM3 is comprised of 10 subsurface soil layers. The oceanic model is based upon the Parallel Ocean

Program version 2.0 (POP2; Smith and Gent, 2002) and uses a grid with a nominal horizontal resolution of 3°. The grids have two poles, one located at the true South Pole and the second over Greenland (Smith et al., 1995). The vertical dimension is treated with 25 layers extending to 4.75 km. The Community Sea Ice Model version 5.0 (CSIM5; Briegleb et al., 2004) is integrated on the same horizontal grid as the ocean model.

4.2 Boundary condition for the Late Permian and Early Triassic

This study employs boundary conditions for the model as summarized in Table A.1 (Appendix A) and are discussed in the following (see Kiehl and Shields, 2005; Winguth et al., 2015). The solar insolation constant (S_0) for the Permian-Triassic boundary was adjusted to 1338 W m^{-2}, which represents approximately a 2.1% decrease relative to the present-day value (based on calculations by Boothroyd; see Caldeira and Kasting, 1992; Winguth et al., 2002) to reflect a fainter sun. To represent equal receipt of solar insolation for both hemispheres, we assume a circular orbit with an eccentricity value of 0°, and Earth's obliquity (axial tilt) at 23.5° (Gibbs et al., 2002). Greenhouse gas concentrations were set to 0.7 ppmv pCH_4, and 0.275 ppmv pN_2O as obtained from Kiehl and Shields (2005; see Tab. 4.1).

Two greenhouse gas levels were considered for the sensitivity experiments to simulate a transition across the boundary. We assume,

24

following Kidder and Worsely (2004), that the Late Permian atmospheric pCO_2 was at 4 x CO_2 relative to preindustrial value (PAL) of 280 ppmv, and that a perturbation massive release of greenhouse gas emissions by Siberian volcanism equivalent to 4,872 Pg C led to a rise in atmospheric pCO_2 of 12.7 x CO_2 PAL at the PTB. Furthermore, reconstructions of greenhouse gas concentrations remain provisional because of the uncertainty encompassing the amount of carbon injection from the Siberian-Trap volcanism (Svensen et al., 2009) and the uncertainty of the atmospheric pCO_2 estimate from paleoproxies (Foster et al., 2017). The 4 x CO_2 simulation represents the Wuchiapingian stage and the 12.7 x CO_2 simulation represents the Changhsingian stage that also marks the end of the Permian period. A third climate sensitivity simulation uses a 12.7 x CO_2 level with thin cloud cover. This portion of the experiment examines the role of cloud albedo in response to a reduction in cloud droplet concentration, following the approach of Kump and Pollard (2008) and Winguth et al. (2015). An increase in CO_2 would decrease marine productivity, reducing the emission of dimethyl sulfide (DMS) or dimethylsulfoniopropriate (DMSP) into the atmosphere (Charlson et al., 1987; Kump and Lovelock, 1995; Lovelock and Kump, 1994). The reduction in DMS concentrations would reduce cloud condensation nuclei and cloud optical depth, further exacerbating global warming (Winguth et al., 2015). This extreme scenario

25

represents a hothouse world assumed for the Early Triassic (combined Induan and Olenekian stages) climate conditions.

Chapter 5

Data Compilation

This study is a collaborative effort to compile lithological and phytogeographic data to identify global distribution patterns to reconstruct a climate transition across the Permian-Triassic boundary (Fig. 5.1; see Appendix C). The compilation and analysis of geologic data for the present study is based on the approach as described by Rees et al. (2002). The compiled data is used for the paleogeographic distribution and quantitative analysis. The lithological database was compiled from previous studies by Rees et al. (2002), the PALEOMAP Project by Scotese (2001), and additional literature. The data selected for analyses encompass the stages from the Late Permian (Wuchiapingian and Changhsingian stages) and Early Triassic (combined Induan and Olenekian stages). The database includes 504 proxies that are classified Upper Permian deposits which include: 91 evaporites, 104 peat/coal, 51 carbonates, 233 reefs, and 25 oil source rocks. The reef database comprising the taxonomic list has been gathered from the Paleobiology Database (www.paleodb.org). There are 84 proxies that are classified as Lower Triassic deposits which include: 42 evaporites, 19 peat/coal, and 23 carbonates. Note that reefs in the Lower Triassic are limited and this period is referred as reef gap, potentially linked

to ocean acidification (Kiessling and Simpson, 2011). The database provides information on current and paleogeographic coordinates, approximate age range of proxy formation and supporting literature references.
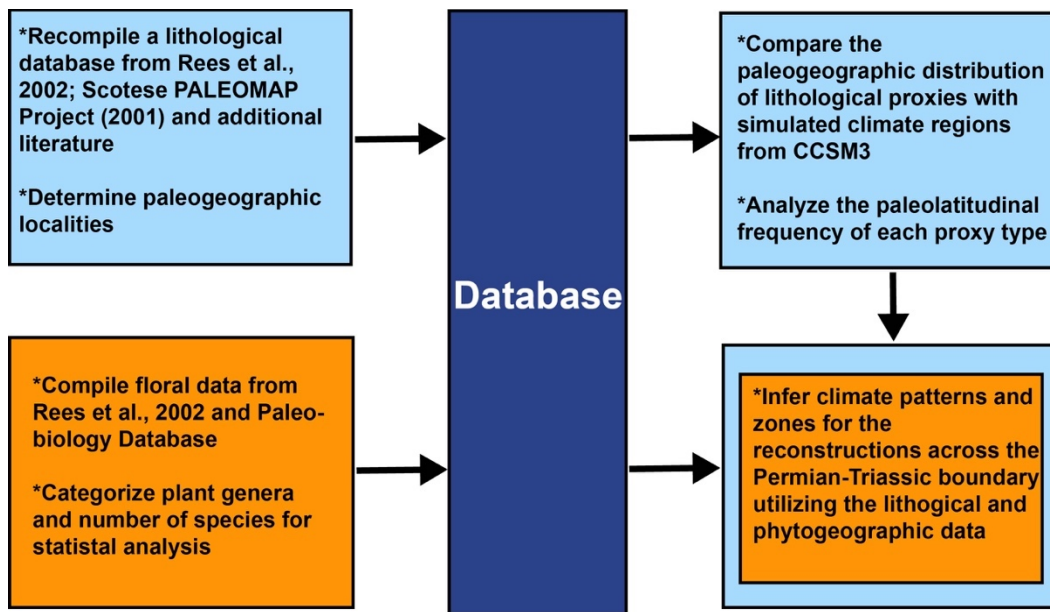
Figure 5.1 Methodology for the reconstruction of climate regions across the PTB (courtesy of Arne Winguth; adapted from Rees et al., 2002).

With the Permian-Triassic boundary in a global state of flux, it is difficult to categorize lithological data into appropriate stages unless the strata contain volcanic ash that can be constrained using first or last appearance fossil datum. The lithological data was categorized as Upper Permian (259.1 - 251.9 Ma) or Lower Triassic (251.9 - 247.2 Ma). The

present-day geographic coordinates for each proxy type were input into an open-source, cross-platform plate tectonic geographic information system, enabling the interactive manipulation of plate-tectonic reconstructions and the visualization of geodata through geological time, GPlates version 2.0 (Müller et al., 2018). Present-day geographic coordinates were transformed via GPlates to paleolocations of the boundaries between the last two Late Permian stages and the first two Early Triassic stages. For the Upper Permian data, we assumed an age of 254.14 Ma which is the boundary between the Wuchiapingian and Changhsingian stages according to International Commission of Stratigraphy (ICS) International Chronostratigraphic Chart of 2020/01 (Cohen et al., 2013). Lower Triassic proxies were assigned an age of a 251.2 Ma (Cohen et al., 2013), which is the boundary age between the Induan and Olenekian stages.

The distribution of lithological proxies was projected on a paleogeographic map of Pangea and compared to climate regions inferred from evaporation and precipitation patterns, sea surface height and temperature from CCSM3 paleoclimate simulations (Winguth et al., 2015). Finally, the distribution and frequency of lithological proxies is analyzed in both hemispheres based on paleo-latitudinal location.

Chapter 6

Results

6.1 Climate pattern inferred from present-day lithological proxies

In the following we discuss present-day correlations between sedimentary deposits and climate patterns. We then apply these correlations to the Permian-Triassic by using data sets described in Chapter 5 and paleoclimate simulation described in Chapter 4.

Evaporites can be representative of arid climate conditions where evaporation exceeds precipitation, where in contrast coal deposits can be representative of humid regions with ever wet conditions. We follow the approach of Ziegler et al. (2003; Fig. 6.1) comparing the occurrence of evaporites and coal to model simulated atmospheric processes.

Reef formation can be dependent on oligotrophic waters that do not exceed critical temperatures thresholds that are imperative to the survival of the symbiotic zooxanthellae that are crucial for the survival of the coral. Because carbonate formation can be influenced by oceanic processes, we focus on the factors that limit coral reef development, including temperature and light penetration to the sea floor. These factors are taken into consideration as we follow the approach of Ziegler et al. (2003; Fig. 6.2) when comparing carbonate formation to model simulated oceanic
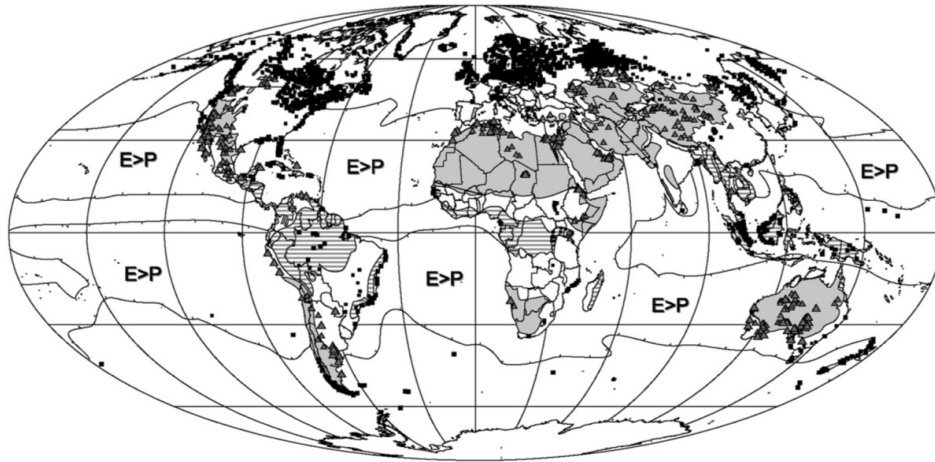
Figure 6.1 Present-day distribution of evaporites (triangles) and peat (squares). Barbed lines indicate regions where evaporation exceeds precipitation (E>P). Adapted from Ziegler et al. (2003).
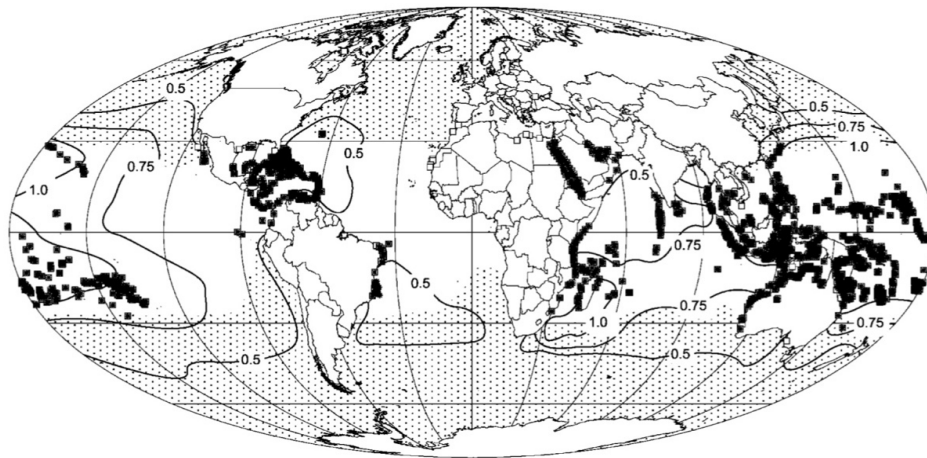
Figure 6.2 Present-day distribution of carbonates (boxes) and reefs (asterisks), with dynamic sea elevation heights and sea surface temperatures. Sea surface elevations of 0.5, 0.75, and 1 m above average (labeled lines), and the low latitude zone where the temperature exceeds 20°C throughout the annual cycle. Adapted from Ziegler et al. (2003).

processes such as, simulated sea surface height (SSH) and sea surface temperature (SST).

A common naming convention is to use the present-day country name that was referenced in the corresponding data sets; however, we will refer to the plotted lithological localities using the corresponding paleogeographic regions (see Tab. B.1 Appendix B; Fig. 1).

6.2 Paleogeographic distribution and frequency of evaporites and coal deposits of across the Permian-Triassic boundary

In the following section, we present the paleogeographic distribution and frequency of evaporite and coal deposits across the Permian-Triassic boundary. The paleogeographic locations of Upper Permian and Lower Triassic lithological proxies are plotted on a paleogeographic map of Pangea and further compared to sensitivity experiments from the CCSM3. Our study includes   Permian evaporite deposits that are distributed across the regions of northern Cathaysia, Cimmeria, eastern and southwestern Euramerica, eastern and central Gondwana (Fig. 6.3). These deposits are largely confined to low and middle latitudes in both hemispheres (Fig. 6.4). In the Northern Hemisphere, evaporites are concentrated between 10° and 20°N across eastern Euramerica. In the Southern Hemisphere evaporite deposits are located within 20° and 30°S in eastern and central Gondwana; however, some of the evaporite deposits that are plotted along the eastern

coast of Gondwana are recorded in the data as present-day Iran, which is not consistent with paleogeographic reconstructions (see Chapter 7); taking this into consideration, the evaporite deposits in this region should be interpreted as Cimmerian evaporite and not identified as eastern Gondwana deposits. Furthermore, the highest latitudinal frequencies of these evaporites in both latitudes coincide with the latitudes of aridity as simulated by the 4 x CO_2 scenario (Fig. 6.4). Evaporites are more prevalent in the Northern Hemisphere during the Late Permian, which could be accounted for by more shallow marine environments in the Northern Hemisphere relative to the Southern Hemisphere.

Lower Triassic evaporite deposits (Fig. 6.5) extend into regions of southern Cathaysia, eastern and southwestern Euramerica and the central and eastern Gondwana. Lower Triassic evaporites are extensive in the Northern Hemisphere between 10° and 20°N in southwestern Euramerica. In the Southern Hemisphere, these deposits are located between 0° and 10°S in southeastern Euramerica (Fig. 6.6). These deposits form a broad belt along the margin of Tethys and are nearly continuous in latitudes from 40° north and 50° south, that may be consistent to a pole-ward expansion
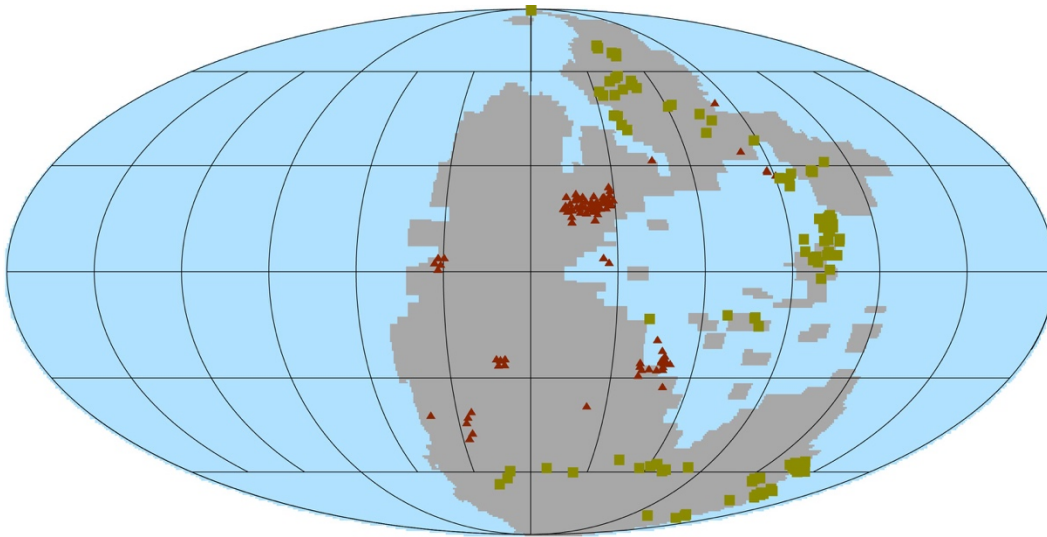
Figure 6.3 Upper Permian evaporites (red triangles) and peat and coal (green squares) are projected onto a paleogeographic reconstruction of Pangea.

of subtropical arid belts in the Early Triassic described by Erwin et al. (2006). Note that the expansion of the subtropics cannot be reproduced by CCSM3. The wide evaporite belts coincide with latitudes that are occupied by the subtropical highs today and infer that they have remained in the same broad bands through long periods of geological time (Ziegler et al., 2003). Furthermore, the geologic data supports the model simulated zonal averages for evaporation minus precipitation for the 4 x CO_2 scenario (Fig 6.6).

Figure 6.4 Paleo-latitudinal frequency of Upper Permian evaporites with simulated evaporation minus precipitation (mm day^{-1}) for the 4 x CO_2 simulation with CCSM3.

The database includes Upper Permian peat and coal deposits that occur in the regions of Angara, northern and southern Cathaysia, Euramerica, and southern Gondwana (Fig. 6.3). In the Northern Hemisphere these deposits are concentrated relative to the equator between 0° and 10°N along the intertropical convergence zone (ITCZ) in southern Cathaysia. Peat and coal in this region are supported by rainfall that is continuous throughout the annual cycle. Coal deposits in southern Cathaysia are plotted within a region where conditions were consistently wet with rainforests (Rees et al., 2002). Peat and coal in low latitudes in the

proximity of the ITCZ are consistent with the model simulated zonal averages of evaporation minus precipitation, where a humid climate is dominant (Fig. 6.7). Coal deposits also occur in wet temperate zones where a humid climate exist. Upper Permian peat and coal deposits extend into high latitudes in both hemispheres and in the Southern Hemisphere coal deposits are recorded between 50° and 60°S in southeastern Gondwana (Fig. 6.7). Furthermore, the coal in this region supports the trend that precipitation exceeds evaporation (Fig. 6.6). Angara and Gondwanan floras of the north and south temperate zones are associated with coal deposits. Evidence of these floras in high latitudes are suggestive of a migration and possible retreat from extreme environmental conditions. Present-day peat and coal of the south temperate latitudes are truncated between 35°N and 55°S simply because the continents terminate at these latitudes. Coal deposits for the Early Triassic are not discussed because of the coal gap (Retallack et al., 1996; see Chapter 7).

In the following, we compare these lithological proxies to the differences in the simulated mean annual precipitation from the mean annual evaporation (P-E) for the 4 x CO_2 simulation, representing the Wuchiapingian (Fig. 6.8), and the 12.7 x CO_2 simulation, representing the Changhsingian stages of the Late Permian (Fig. 6.9). The Lower Triassic lithological proxies are compared to simulated P-E for 12.7 x CO_2 WC with
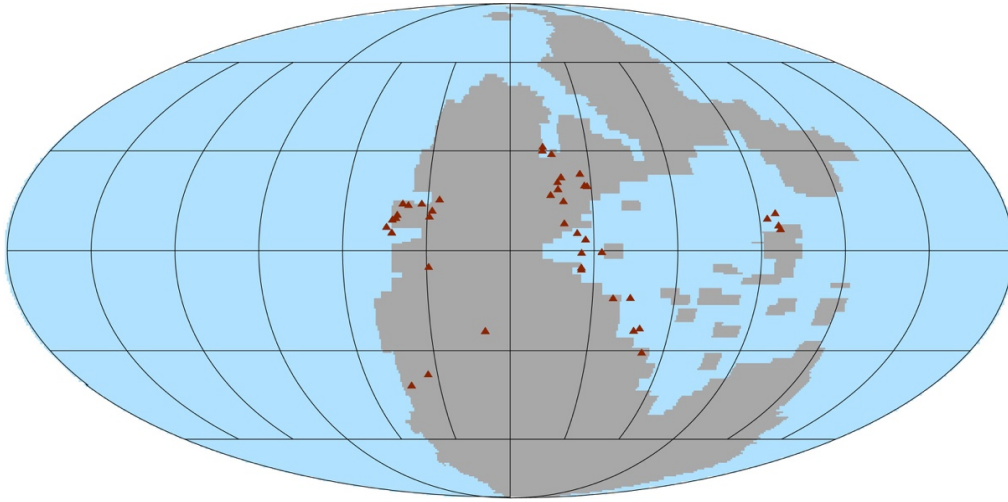
Figure 6.5 Lower Triassic evaporites (red triangles) are projected onto a paleogeographic reconstruction of Pangea. Note coal data are not shown because of the goal gap in the Early Triassic (see Chapter 7).
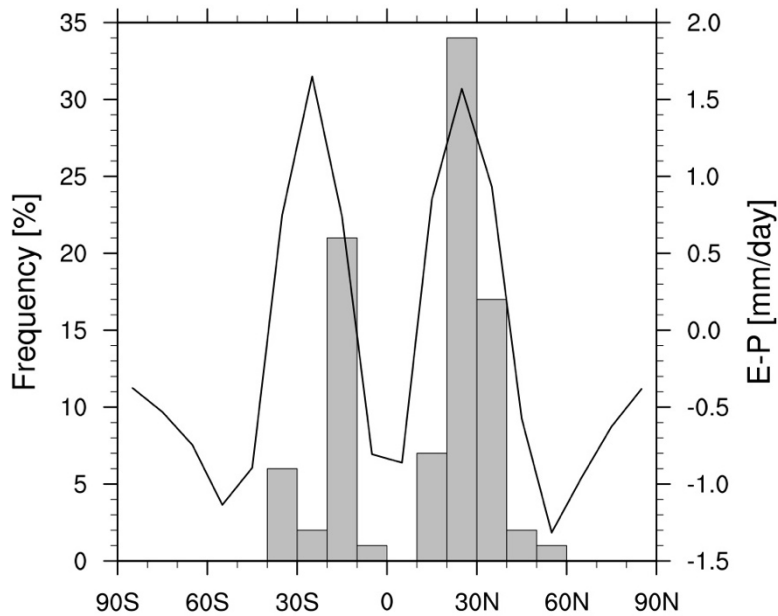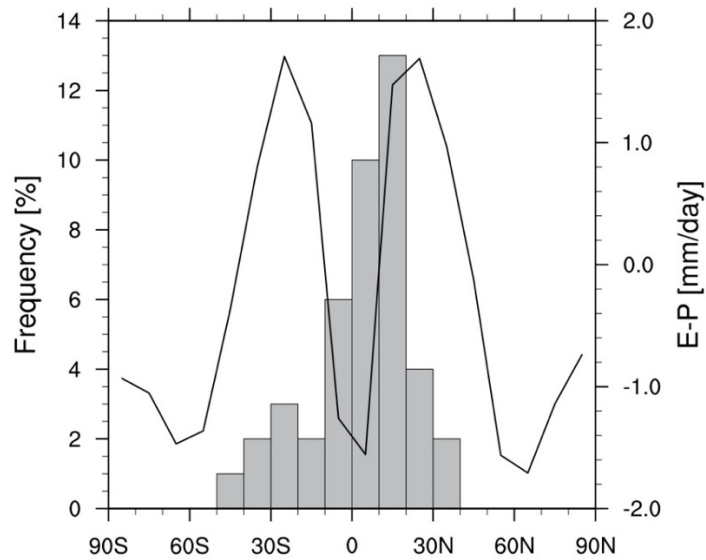

Figure 6.6 Paleo-latitudinal frequency of Lower Triassic evaporites with simulated evaporation minus precipitation (mm day^{-1}) for the 12 x CO_2 WC simulation with CCSM3.
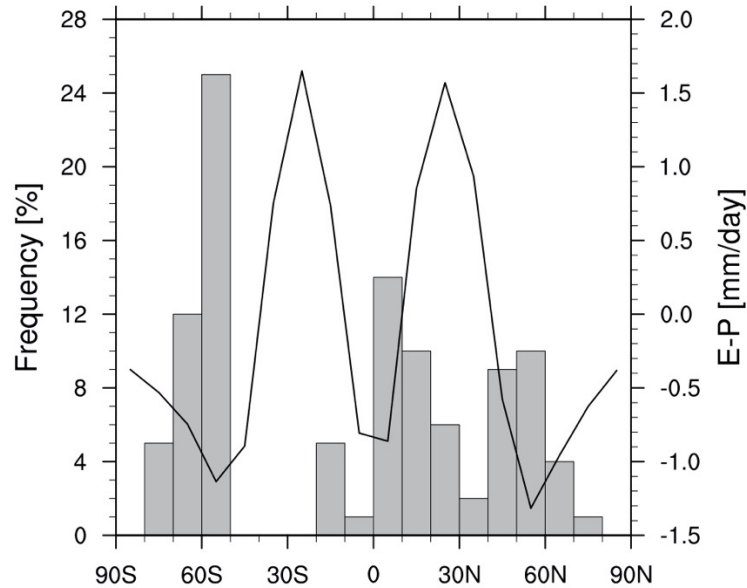
Figure 6.7 Paleo-latitudinal frequency of Upper Permian peat and coal with simulated evaporation minus precipitation (mm day^{-1}) for the 4 x CO_2 simulation with CCSM3.

a thin cloud cover, representing the Early Triassic Induan and Olenekian stages (Fig. 6.10). There is a simulated decrease in precipitation across Pangea when comparing the P-E for the 4 x CO_2 and 12.7 x CO_2 WC scenarios (Figs. 6.8, 6.10). According to these figures vast areas of Pangea are arid to semiarid with evaporation exceeding precipitation over most of the continental interior, consistent with the findings of Kutzbach and Gallimore (1989). These results correlate well with the evaporites plotted within the continental interior of Euramerica and Gondwana where

38

differences do not exceed 1 mm day^{-1} to 2 mm day^{-1}. In southwestern Euramerica a transition from a dominant humid climate to an arid climate has been simulated which corresponds well with the evaporite deposits along the southwestern coast. In eastern Gondwana, evaporation exceeds precipitation by 2 mm day^{-1} and 3 mm day^{-1} which are consistent to the evaporite deposits along the southeastern coast. The extensive evaporite deposits in the Upper Permian suggest an exceptionally dry period and the patterns of P-E indicate aridity between 40°N and 40°S suggesting that major arid zones extended poleward to middle latitudes. In a transition to warmer climate a poleward shift of the tropospheric jet streams and their associated subtropical dry zones may shift poleward (Fu et al., 2006). The high aridity in the Early Triassic stages is supported by evaporite deposits across Pangea and are extensive in southwestern Euramerica. The formation of evaporites in these regions are consistent with low available atmospheric moisture content and aridity due to continentality in the interior (Ziegler et al., 2003). Parrish et al. (1982) discusses extreme monsoonal circulation that would have made the equatorial region very dry and maximized seasonality along the coastal regions of the Tethys. Deviations of evaporates from the zonal models might be accounted for by monsoonal influence since it has the greatest perturbation effect on latitudinal climate zones; however, there are only minor discrepancies in evaporite distribution

compared to the present-day climate, and these may be attributed to variations in paleogeographic reconstructions, etc. Across the Late Permian, the interpreted evaporite belts within the continental interior of Pangea demarcate the coal belts in higher latitudes.

Across both Latest Permian stages, the simulated precipitation exceeds evaporation for the 4 x CO_2 and 12.7 x CO_2 scenarios (Figs. 6.8, 6.9). Analysis of differences between precipitation and evaporation for the 12.7 x CO_2 and 4 x CO_2 simulation suggest that precipitation in the Northern Hemisphere exceeds that of the Southern Hemisphere due to higher continentality in the later and dominant marine influences in the former (Figs. 6.8, 6.9). The differences near the ITCZ range from 4 mm day^{-1} to 8 mm day^{-1}. In southern Cathaysia P-E is 2-5 mm day^{-1} and increases in the Early Triassic scenario by 1 mm day^{-1}. These findings are consistent with the peat and coal deposits in southern Cathaysia and areas of simulated rise of humid climates over the Tethys along the ITCZ in regions where conditions were consistently wet with rainforests (Rees et al., 2002). Peat-forming swamps in the coastal regions are suggestive of the continuity of precipitation through the annual cycle (Lottes and Ziegler, 1994) and therefore of fresh-water runoff and stratified water masses. when increases latitudinally over the ITCZ (Figs. 6.10, 6.8). While the ITCZ comparing the
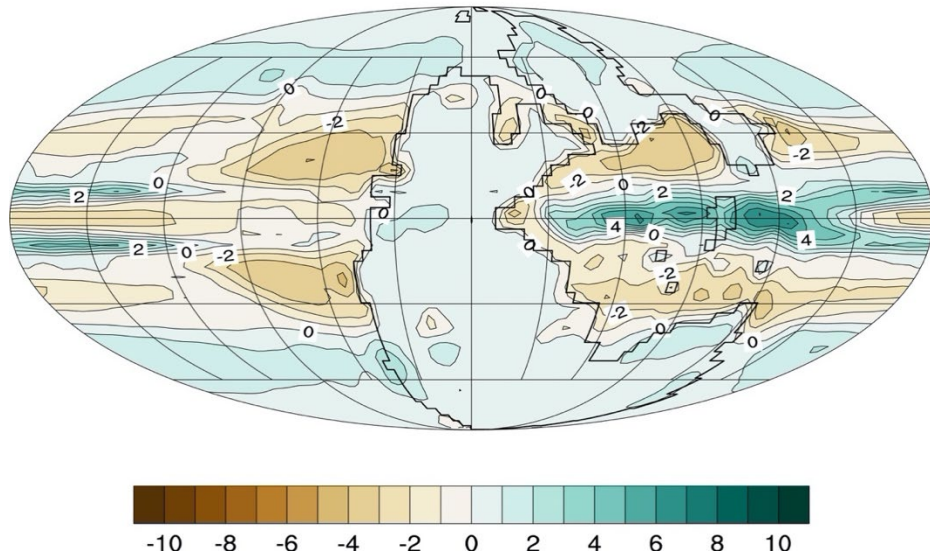
Figure 6.8 Total annual precipitation minus evaporation (mm day^{-1}) for the 4 x CO_2 simulation with CCSM3.
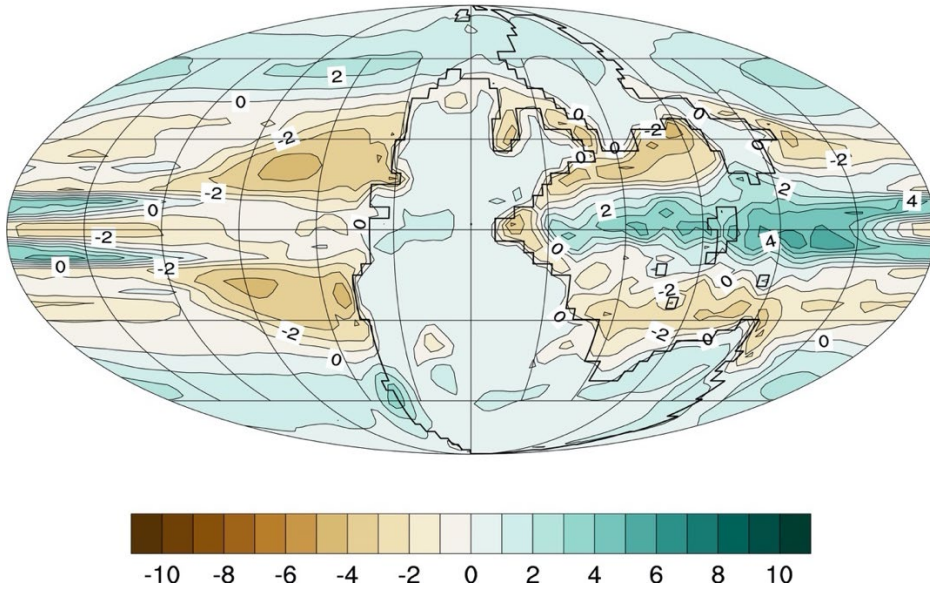
Figure 6.9 Total annual precipitation minus evaporation for the 12.7 x CO_2 simulation with CCSM3.
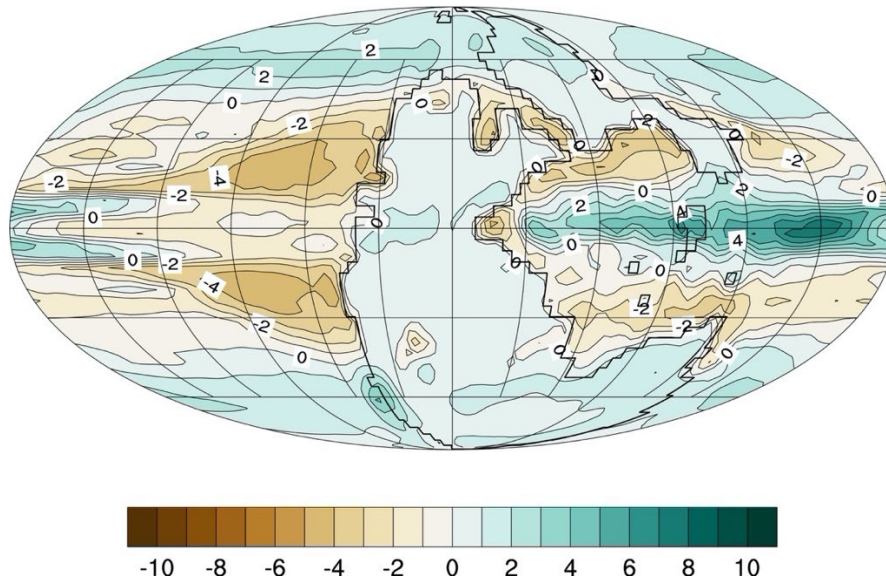
Figure 6.10 Total annual precipitation minus evaporation (mm day^{-1}) for the PTB 12.7 x CO2 WC simulation with CCSM3.

12.7 x CO$_2$ WC and 4 x CO$_2$ scenarios, precipitation dominates the coal deposits within 10° of the equator, higher latitudes support coal deposits in wet temperate zones. In middle to high latitudes, an increase in humid climate (P>E 1 mm day^{-1} to 3 mm day^{-1}) across the PTB over the ocean and land is in general agreement with the patterns of the lithological deposits in southern Gondwana.

6.3 Paleogeographic distribution and frequency of carbonates and reef deposits of across the Permian-Triassic boundary

In this section the paleogeographic distributions of carbonate and reef deposits are compared to CCSM3 climate simulations. Upper Permian carbonates are distributed in regions of Angara, southern Cathaysia, eastern Euramerica, and eastern Gondwana (Fig. 6.11). In the Northern Hemisphere these deposits occur mostly between 10° and 20°N in eastern Euramerica (Fig. 6.12). Carbonates are located within 20° and 30°S in eastern Gondwana may be rather assigned to be Cimmerian carbonate deposits; the reason for these differences are uncertainties in the paleolocalities since the samples originates from present-day Iran (see Chapter 7). Carbonate deposits within these regions correlate well with the simulated high-pressure zones and surface air temperatures above 20° C as simulated for the 4 x CO_2 scenario from CCSM3 (Fig. 6.12). These findings are fairly consistent with enhanced calcium carbonate production in warm waters.
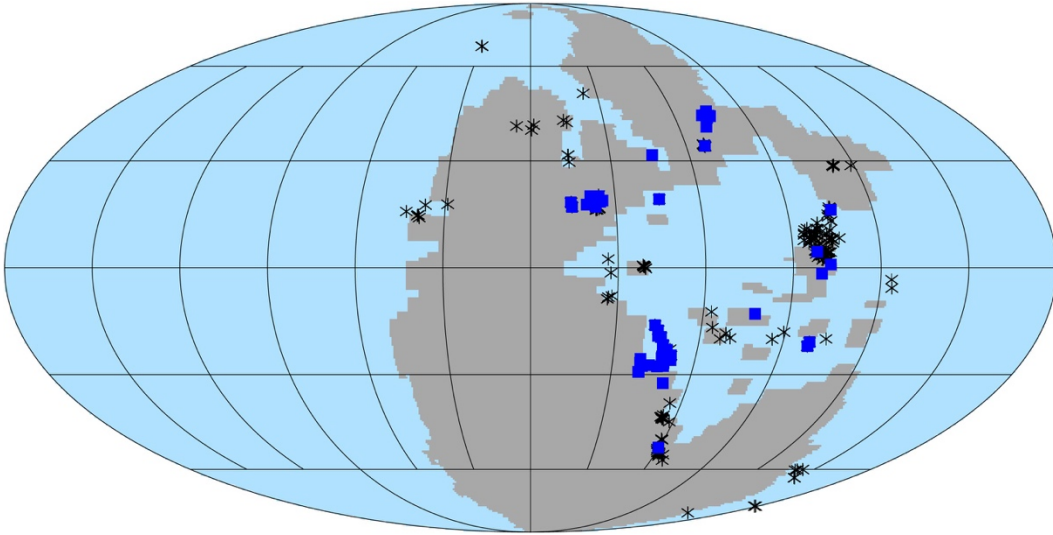
Figure 6.11 Upper Permian carbonates (blue squares) and reefs (asterisks) are projected onto a paleogeographic reconstruction of Pangea.
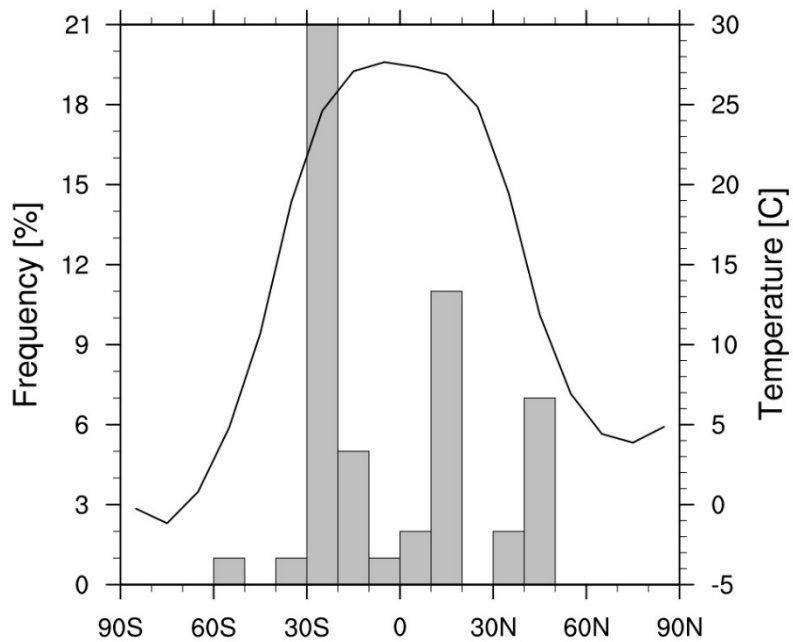
Figure 6.12 Paleo-latitudinal frequency of Upper Permian carbonates with simulated surface air temperature (SAT, in °C) for the 4 x CO2 simulation with CCSM3.

Lower Triassic carbonates are distributed throughout regions of eastern Euramerica, and south central Gondwana (Fig. 6.13). In the Northern Hemisphere, these proxies are centrally located between 10° and 20°N in eastern Euramerica. In the Southern Hemisphere, carbonate rocks are prevalent in higher latitudes between 60° and 70°S in south central Gondwana (Fig. 6.14). The carbonates recorded in higher latitudes indicate and expansion of warmer temperatures in the polar regions which is supported by the 12 x CO_2 WC simulation. Limestone deposition may depend to a certain degree on water masses that have a sufficient high temperature; however, the rate and extent of terrigenous sediment dilution appears to be the primary factor that determine limestone deposition at nearshore or continental shelf depths.

Upper Permian reefs occur in regions that coincide with carbonate deposits and plot similar due simply to reefs being the most obvious element of the carbonate system, so that there is an inherent bias at the data assembly level. These proxies are distributed in regions of southern Cathaysia, eastern Euramerica, and eastern Gondwana (Fig. 6.11). In the Northern Hemisphere these deposits are mostly concentrated between 10° and 20°N in the Tethys (Fig. 6.15). In the Southern Hemisphere reefs
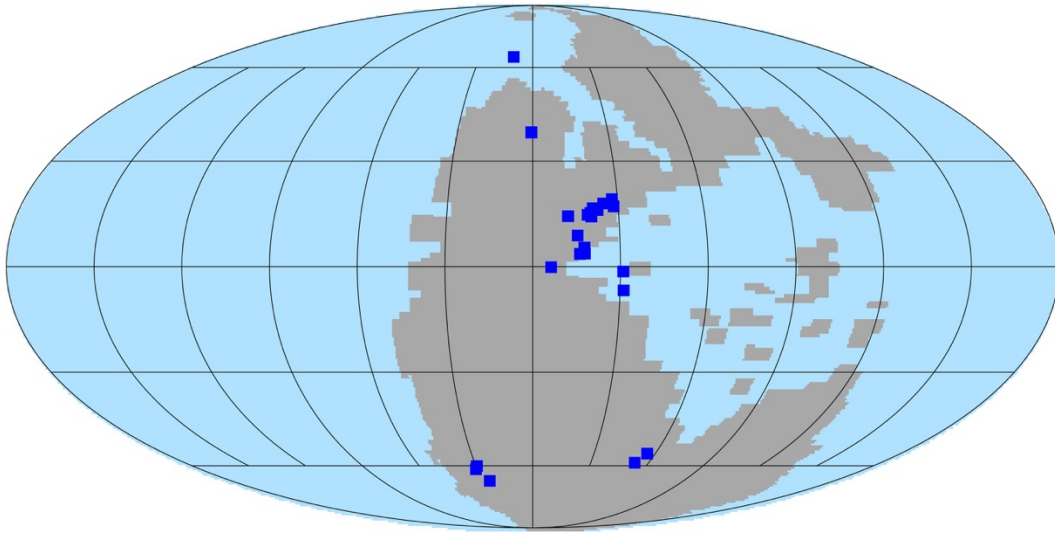
Figure 6.13 Lower Triassic carbonates (blue squares) are projected onto a paleogeographic reconstruction of Pangea. Note there are not sufficient reef data available for the early Triassic (reef gap; see text).
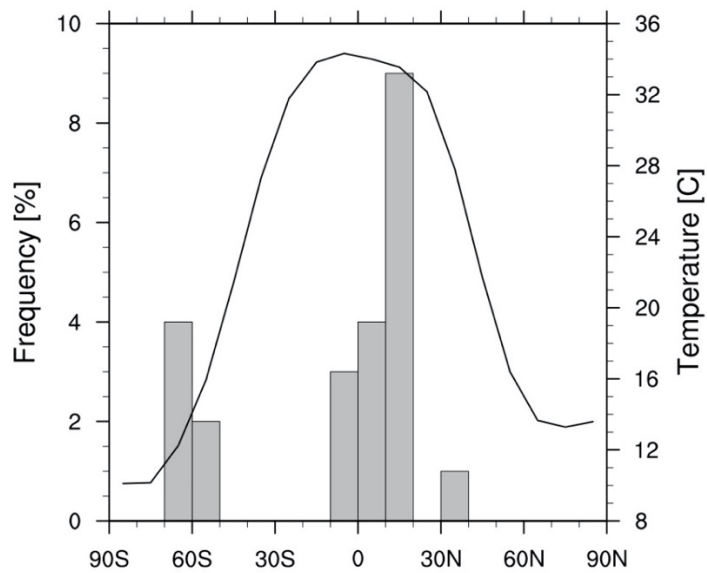
Figure 6.14 Paleo-latitudinal frequency of Lower Triassic carbonates with simulated surface air temperature (SAT, in °C) for the PTB 12.7 x CO2 WC simulation with CCSM3.
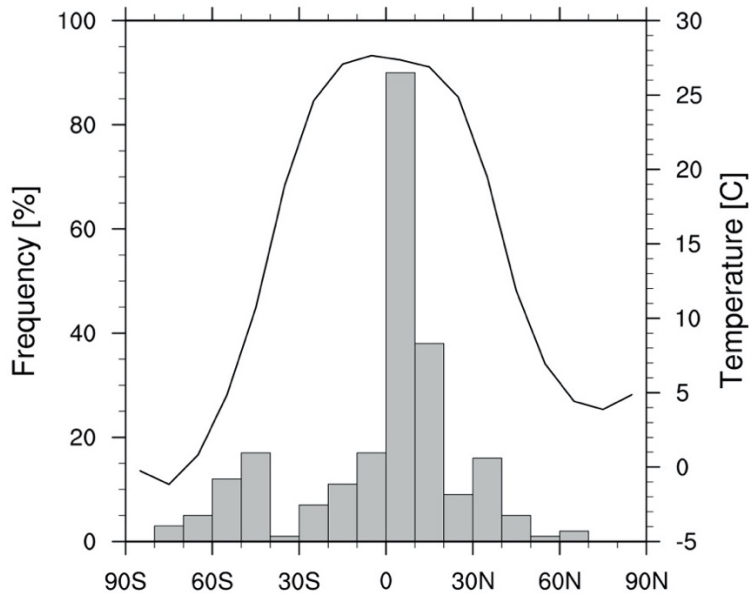
Figure 6.15 Paleo-latitudinal frequency of Upper Permian reefs with simulated sea surface air temperature (SAT, in °C) for the 4 x CO2 simulation with CCSM3.

are concentrated between 40° and 50°S in southeastern Gondwana. Upper Permian reefs occur in subtropical regions whereas equatorial regions are characterized by Ekman-induced upwelling of cool water masses, high rainfall associated with ITCZ, and high surface runoff from adjacent coastal regions (Ziegler et al., 2003). Cooler water and upwelling favor productivity which impedes light penetration. The frequency of Upper Permian reefs in low latitudes of the Northern Hemisphere, coincide well with the model simulated zonal mean sea surface temperature above the 20°C isotherm for the 4 x CO_2 scenario from CCSM3 (Fig. 6.15). Distributions of the early

47

Triassic reefs are not discussed because the lack of available data associated with the reef gap linked to extreme environmental stress (hot temperature and ocean acidification; see Kiessling and Simpson, 2011, and Ziegler et al. 2003).

In the following, we will discuss the corresponding PTB climate simulations with focus on temperature change and sea surface height. Differences in sea surface height in the Tethys do not vary substantially from the Permian to the Triassic as inferred from differences between the 12.7 x CO_2 experiment and the 4 x CO_2 experiment (Fig. 6.16), representing changes in the latest Permian, and differences between 12.7 x CO_2 WC scenario and the 4 x CO_2 (Fig. 6.17) scenario, representing changes from the latest Permian to the earliest Triassic. Ziegler et al. (2003) suggest that areas of highs in sea surface height, representing regions of high solar radiation and Ekman convergence, and warm sea surface temperature >20°C may be suitable conditions for abundant reef deposits. Since reef deposits (Fig. 6.11) have been mostly centered in the Tethys realm one could infer that the changes in sea surface height did not contribute substantially to the reef gap in this region. The difference in simulated sea surface height exceeds 20 cm along the eastern coast of northern Cathaysia which corresponds with a difference in sea surface temperatures exceeding 9°C (Fig. 6.16). The coastal polar regions of western Pangea

simulate a difference in sea surface height of approximately 20 cm. Similarly, the difference in sea surface temperatures in this region is approximately 1°C. The simulated difference in sea surface temperature along the equatorial region is 3°C -4°C.

The difference between the 12.7 x CO_2 WC scenario and 4 x CO_2 (Fig. 6.17) scenario exceeds 30 cm along the eastern coast of northern Cathaysia. This difference is correlated with changes in sea surface temperatures that exceeds 12°C in this area. The coastal polar regions of western Pangea simulate a difference of approximately 20 cm consistent with the 4 x CO_2 scenario. Similarly, the difference in sea surface temperatures in this region is approximately 5-6°C. There is an increase in simulated difference in sea surface temperature along the equatorial region is 6-8°C relative to the pre-PTB conditions. When comparing the differences in simulated sea surface temperatures across the boundary, we see the eastern Gondwana carbonates favor formation in regions with a relatively slight difference in sea surface temperatures. Shallower depth in the eastern Panthalassa can be attributed to upwelling of subsurface water masses and Ekman transport producing variations in the sea surface height; although we do have not fully incorporated carbonate data along the western coast of Pangea, this upwelling region is comparative to regions that favor reef formation which we discuss later.
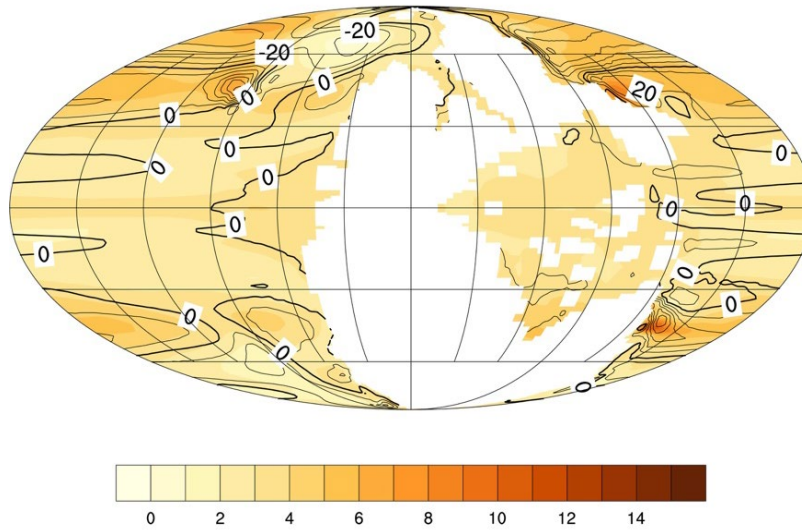
Figure 6.16 Difference in simulated sea surface height (SSH, in cm) and sea surface temperature (SST, in °C) for 12.7 x CO_2 scenario minus 4 x CO_2 scenario. Contour lines from -60 cm to 60 cm with interval of 10 cm.
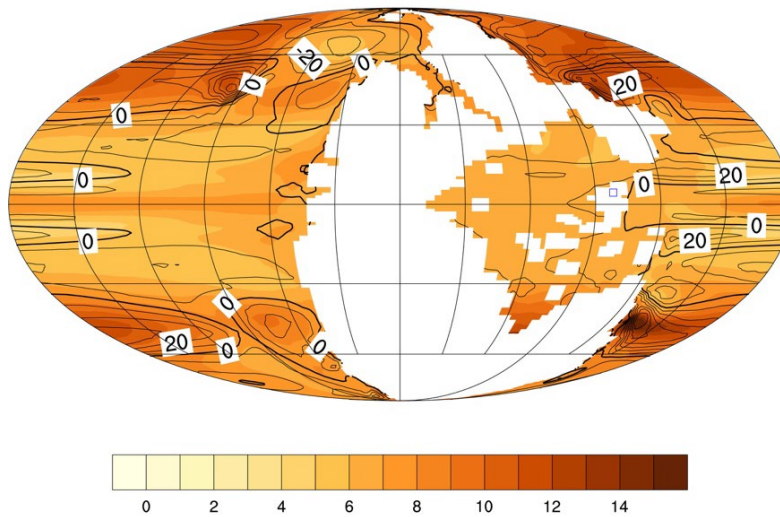
Figure 6.17 Difference in simulated sea surface height (SSH, in cm) and sea surface temperature (SST, in °C) for 12.7 x CO_2 scenario minus 4 x CO_2 scenario. Contour lines from -60 cm to 60 cm with interval of 10 cm.

Chapter 7

Discussion

The sensitivity experiments presented in this study exemplify potential feedbacks in the climatic transition from a greenhouse to a hothouse climate during the end Phanerozoic (Winguth et al., 2015). Siberian volcanism (Renne and Basu, 1991; Renne et al., 1995; Kamo et al., 2003; Svensen et al., 2009), coal bed intrusions (Retallack and Jahren, 2008), and forest fires (Hudspith et al., 2014) associated with coal-fly ash deposits (Nestell et al., 2015) would have resulted in a significant influx of carbon into the atmosphere (Svensen et al., 2009; Retallack et al., 2011; Brand et al., 2012) that potentially induced a climatic warming (Hallam and Wignall, 1997; Kidder and Worsley, 2010; Joachimski et al., 2012; Sun et al., 2012; Schobben et al., 2014) across the Permian-Triassic boundary.

For this study, we consider two greenhouse gas levels that were considered for the sensitivity experiments to simulate a transition across the boundary. We follow Kidder and Worsely (2004), by assuming that the Late Permian atmospheric pCO_2 was at 4 x CO_2 relative to preindustrial value (PAL) of 280 ppmv, and that a perturbation massive release of greenhouse gas emissions by Siberian volcanism equivalent to 4,872 Pg C led to a rise in atmospheric pCO_2 of 12.7 x CO_2 PAL at the PTB. The reconstructions of

greenhouse gas concentrations remain not well determined because of the uncertainty encompassing the amount of carbon influx from Siberian volcanism (Svensen et al., 2009) and the uncertainty of the atmospheric pCO_2 estimate from paleoproxies (Foster et al., 2017). Our results yield differences in simulated sea surface temperature of 3-4°C (equivalent to an atmospheric increase of 5000 Pg C) across the simulated Wuchiapingian (4 x CO_2) and Changshingian (12.7 x CO_2) stages. In addition, Joachimski et al. (2012) inferred a warming of ~8°C in the Tethys Ocean. According to Svensen et al. (2009), it was possible to have an atmospheric increase of more than 5000 Pg C in the Early Triassic.

Another crucial boundary condition is the continental positioning for climate modeling and more uncertainties exist with this condition the farther back the reconstructions occur in deep geologic time. Although the configuration of Pangea is reasonably consistent regarding modeling reconstructions, the positions of the southeastern Asian microplates in the Tethyan realm are more uncertain (Gibbs et al., 2002). Some discrepancies exist between plotted lithological data and the simulated configuration of Pangea. The coastlines are not well resolved, which could account for why some marine/terrestrial deposits appear onshore/offshore (e.g. southeastern Gondwana, northern Cathaysia, and eastern Euramerica). These discrepancies may also be accounted for by the fact that CCSM3

52

does not simulate a continental drift of Pangea or the Cimmerian microcontinents across our boundary experiments; although, it does not seem plausible that the rate of plate movement would be substantial enough to account these small errors. The most uncertainties regarding paleocoordinates are associated with the Cimmerian lithological data, particularly regarding the present-day regions of Iran, Tibet, Turkey, and Vietnam. Following the latest plate tectonic reconstructions, some of this data is off by approximately 10° in latitude and/or longitude which can account for a misinterpretation of data and inferred climate regions; therefore, we attempt to isolate global patterns based on the frequency of the lithological distributions. Uncertainties in the paleocoordinates of the lithological data could be attributed to incorrect assignment of plate IDs within GPlates or the application of a uniform age for all proxy data when determining paleocoordinates. In addition, some disagreements may arise in the classification of data as Upper Permian or Lower Triassic because the boundary is in a global state of flux and may be incomplete or poorly constrained in some localities unless the strata contains volcanic ash deposits, or first or last appearance fossil datum.

In addition, all factors regarding lithological formation must be considered when utilizing lithological data as proxies to infer global climate patterns. The formation of sedimentary rocks is largely controlled by

atmospheric and oceanic processes that are considerably consistent; however, the formation of some rock types are not always dependent on the same physical or geochemical factors and these factors need to be noted when regarding generalized climatic interpretations, as the formation of some proxies may be a result of regional and not global effects. The extensive evaporite deposits in the Upper Permian suggest an exceptionally dry period and some authors have been tempted to correlate broad evaporite basins with this dry period; however, Ziegler et al. (2003) argues that there is an inherent bias regarding the lithological data because of the broad epeiric basins located in subtropical latitudes of Euramerica. Ziegler et al. (2003) also notes that desert deposits that are typical of the continental interior are less likely to be preserved in the geologic record. Kozary et al. (1968) notes that the only Paleozoic evaporites that still exist are those which were formed in intracratonic basins. Algeo et al. (2011) argues that extinction event studies have been focused on marine records because they are more stratigraphically complete and likely to preserve globally integrated signals compared to terrestrial records; therefore, interpreting climate changes in regions over the continental interior with low preservation of may be limited.

Coal formation is prevalent along the equatorial regions near the intertropical convergence zone (ITCZ) where precipitation is continuous

throughout the annual cycle; however, other important rain-producing systems include the orographic and diurnal land-sea systems (Gyllenhaal et al., 1991) influence the formation of peat and coal as seen in upland peat deposits on mountainsides in deserts as a result of regular orographic precipitation. Peats also form in mangrove swamps, which derive moisture from the seawater, not rainfall; however, mangrove peats are well developed in areas with the highest precipitation (Woodroffe et al., 1992); therefore, caution should be taken when inferring climate patterns based on precipitation patterns regarding these lithological proxies. Furthermore, Parrish et al. (1982) suggests that the most reliable test of the rainfall maps would be those that compare the patterns with paleo-phytogeographical patterns across the boundary. An extensive comparison is outside the scope of this study and one refer the reader to other studies (see e.g. Ziegler et al., 1998; Rees et al., 1999; Rees et al., 2002; Gautam et al., 2019). We do not discuss Lower Triassic coal data because of the Early to Mid-Triassic "coal gap" (Retallack et al., 1996) that is recognized with the disappearance of the coal swamps of the tropical and temperate zones at or about the end of the Permian period (Ziegler et al., 2003). Approximately 95% of peat-producing plants went locally extinct at the boundary (Michaelsen, 2002). The lack of coals in the geologic record may be attributed to their migration to regions that did not preserve an Early Triassic sedimentary record rather

than a disappearance of coal-producing ecosystems (McElwain et al., 2007). *Vertebraria-* and *Glossopteris-* dominated floras were last recorded in eastern Australia for 5-10 Myr before peat-forming ecosystems reestablished in the Middle Triassic (Retallack et al., 1996). Moreover, floras are documented in high latitude regions, which implicated a retreat from lower latitude critical temperature thresholds to "cooler" polar latitudes. Rees et al. (2002) argued the extinction of peat-forming plants are a result of regional not global effects.

Discrepancies occur with the plotted carbonate data within the continental regions of Pangea, which is a discrepancy related to the reconstruction of paleocoordinates and/or the paleogeographic reconstruction of Pangea; therefore, caution should be taken when interpreting these proxies to simulated oceanic factors. Lower Triassic carbonates are recorded in higher latitudes which indicate an expansion of warmer temperatures in the polar regions; however, the rate and extent of terrigenous sediment dilution appears to be the primary factor that determine limestone deposition at nearshore or continental shelf depths. Moreover, a common misconception is that a warm water environment is essential for limestone formation and although calcium carbonate productivity is lowest in cold climates, cool-water carbonates can form in ocean temperatures between 10-16ºC (Leonard et al., 1981) and

carbonates in cool water environments have long been recognized (James, 1997).

Modern reef and carbonate plots are similar due simply to reefs being the most obvious element of the carbonate system, so that there is an inherent bias at the data assembly level. The number of modern reefs is high and should provide a cautionary note concerning the reliability of the fossil record of reefs. In addition, the database lacks Lower Triassic reef records because there was an annihilation of reef-building organisms at the end of the Permian followed by an absence of platform margin reefs during the Early Triassic, 5-6 Myr (Martin et al., 2001; Mundil et al., 2004). This extinction determined the disappearance of tabulate and rugose corals from reef ecosystems (Hallam and Wignall, 1997). Corals did not recover until the Middle Triassic when scleractinians emerged (Pruss and Bottjer, 2005). Because of the absence of metazoan reef builders, the Early Triassic has been dubbed a 'reef gap' (Fagerstrom, 1987); the "reef gap" in the Early Triassic, is parallel with the coal gap of the terrestrial realm (Zeigler et al., 2003). The acceptance of a 'reef gap' has been revisited with the discovery Early Triassic build-ups that are limited to domal and conical stromatolites and thrombolites (Baud et al., 2007). Although Early Triassic patch reefs are globally documented, we do not include this data in the present study; however, it must be mentioned that microbial patch reefs are documented

in South China (Lehrmann, 1999; Lehrmann et al., 2003), southern Turkey, Armenia, Iran, Oman (Baud et al., 1997; Baud et al., 2002), Greenland (Wignall and Twitchett, 2002), and western North America (Pruss and Bottjer, 2004). The replacement of metazoan reefs by microbial reefs has been interpreted by to represent long-term stressful conditions associated with the end-Permian extinction (Hallam, 1991; Lehrmann et al., 2001; Lehrmann et al., 2003). Sea surface temperatures typically exceeding 30°C may lead to environmental stress and diseases on coral system but some coral species are tolerant to higher temperatures. Zooxanthellae, which live in symbiosis with the corals, may decline in population due to environmental stress which could lead coral bleaching. An increase in sea surface temperatures of 1°C can cause stress on zooxanthellae and coral bleaching (Glynn, 1993). Sea surface temperatures difference between the Early Triassic climate 12.7 x CO_2 WC scenario and the Late Permian 4 x CO_2 scenarios exceeded 5°C in the Tethys. The increase in greenhouse radiative forcing could have provoked global warming and increased tropical sea surface temperatures that were critical to marine biota (Winguth et al., 2015). The Early Triassic scenario supports the hypothesis that temperature thresholds exceeded the minimum values that would cause stress on zooxanthellae and coral bleaching which would have endangered the survival of reef-building organisms. These findings are consistent with

$\delta^{18}O_{apatite}$ values from conodonts that there was an increase in sea surface temperatures from 21 to 36°C and potentially exceeded 40°C by the Early Triassic (Sun et al., 2012). In both hemispheres, sea surface temperature differences were amplified in polar regions. Manabe and Wetherald (1980) suggested that large-scale monsoonal circulation could contribute to a substantial poleward transported. The simulation with reduced cloud albedo (12.7 x CO_2 WC) produced amplification in sea surface temperatures which can be explained by the substantial influence that clouds have on polar energy budgets (Sloan and Pollard, 1998; Kiehl and Shields, 2013; Upchurch et al., 2015) and temperature amplification (Winton, 2006; Kay et al., 2012). The Early Triassic shows temperatures that are in excess of modern equatorial annuals sea surface temperatures (Shen et al., 2011). These simulated temperature thresholds can present a case for lack of reef-building metazoans across the boundary.

Furthermore, increasing carbon dioxide concentrations lowers the oceans pH resulting in ocean acidification. Although the impact of low pH on coral reefs continues to be examined, decreases in pH can reduce the calcification rates of corals and other calcifying organisms (Reis et al., 2009). The sharp increase in atmospheric CO_2 has changed the carbonate chemistry of the surface oceans (Sabine et al., 2004). Since the pre-industrial revolution, model estimates suggest that the average surface

ocean pH has decreased by 0.1 units, which corresponds to an increase in the hydrogen ion concentration and acidity by 25% (Orr et al., 2005; Doney et al., 2009). Sea surface seawater pH may decrease by 0.3-0.4 units by the end of this century (Caldeira and Wickett, 2003; Orr et al., 2005). Major changes in ocean chemistry pose concerns for corals and reef-building ecosystems (Kleypas et al., 1999). An increase in dissolved CO_2 concentration is inevitably linked to ocean acidification, with the following equation:

$$CO_2 + H_2O + CaCO_3 \Leftrightarrow Ca^{2+} + 2HCO_3^- \text{ (eq. 1)},$$
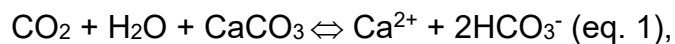
and greater rates of $CaCO_3$ dissolution within the carbonate framework of coral reefs (Yates and Halley, 2006; Manzello et al., 2008). A more acidic ocean may lead to preferential extinction of heavily calcified taxa and other signals in the rock record (Payne et al., 2010). Marine calcifiers would have difficulty depositing skeletons made of $CaCO_3$ under lower seawater pH conditions (Kroeker et al., 2013); furthermore, the dissolution of $CaCO_3$ under these conditions are likely to increase (Andersson et al., 2009; Tribollet et al., 2009). Analyzing the simulated pH with Lower Triassic carbonates and the lack of reefs may further highlight the environmental stresses during Early Triassic. In addition, the model does not distinguish between warm-water and cool-water carbonates, and between different biogeochemical processes that may led to coral bleaching.

60

Chapter 8

Conclusion

In this study, we have compared the Upper Permian to Early Triassic lithological proxies to sensitivity experiments from the Community Climate System Model 3.0. The patterns of climate model simulations across the boundary correlate reasonably well with those from the geological record; however, the model cannot explain the warm polar conditions and the poleward expansion of the subtropical latitudes as potentially revealed from the sedimentary record. This is likely due to missing biophysical feedbacks associated with clouds as suggested in e.g. Kump and Pollard (2008). Evaporites are concentrated within middle latitudes and correlate to regions where simulated evaporation exceeds precipitation with moderately low rainfall. Coal deposits of high latitudes correspond with regions where simulated precipitation exceeds evaporation, although model-data biases in the interior of the continents remains. The lack of Early Triassic reef data is supported by simulated temperature extremes that would have exceeded thresholds critical to marine biota. Hostile climate conditions that culminated in the end-Permian extinction find parallels in the past two centuries affected by widespread deforestation, decline in biodiversity, anthropogenic-induced climate change, and ocean acidification. Hence the signature of physical climate change and exceptional extinction rates at the PTB may provide

61

lessons for future changes. Quantifying these environmental thresholds and defining the drivers of climate changes are of importance in understanding the biotic responses to abrupt anthropogenic-induced global warming.

Appendix A

Boundary Conditions

Table A.1. Boundary conditions for the PTB simulations (adapted from Kiehl and Shields (2005) and Winguth et al., (2015)).

Experiments	Atm. CO_2 conc. (ppmv)	CH_4 (ppmv)	N_2O (ppmv)	S_0 (Wm^{-2})	Eccentricity	Obliquity (degrees)	CDNC (cm^{-3})
4 x PAL CO_2	1120	0.7	0.275	1338	0	23.5	400
12.7 x PAL CO_2	3550	0.7	0.275	1338	0	23.5	400
12.7 x PAL CO_2 WC	3550	0.7	0.275	1338	0	23.5	50
*Note: PAL is Present Atmospheric Level (280 ppmv)							

Appendix B

Paleogeographic Regions

Table B.1 Paleogeographic regions of Pangea with associated the present-day region.

PALEOGEOGRAPHIC REGION	PRESENT-DAY REGION
Angara	Russia Siberia
China	North China South China
Cimmeria	Afghanistan Iran Tibet Turkey Vietnam
Euramerica	Europe North America
Gondwana	Africa Antarctica Australia India Saudi Arabia South America

Appendix C

Database of Lithological Proxies

Table C.1 The lithological proxies were compiled from previous studies by Rees et al. (2002), the PALEOMAP Project by Scotese (2001), and additional literature. The data selected for analyses encompass the stages from the Late Permian (Wuchiapingian and Changhsingian stages) and Early Triassic (combined Induan and Olenekian stages). The database includes 504 lithological proxies that are classified as Upper Permian deposits and include: 91 evaporites, 104 peat and coal, 51 carbonates, 233 reefs, and 25 oil source rocks. The Lower Triassic database includes 84 lithological proxies which include: 42 evaporites, 19 peat and coal, and 23 carbonates. The database provides information on current and paleogeographic coordinates, approximate age range of proxy formation, and supporting literature references. The lithological database is included in the supplemental documents for the thesis and is available at the University of Texas at Arlington library (https://libraries.uta.edu).

References

Algeo, T.J., Chen, Z.Q., Fraiser, M.L., and Twitchett, R.J., 2011, Terrestrial–marine teleconnections in the collapse and rebuilding of Early Triassic marine ecosystems: Palaeogeography, Palaeoclimatology, Palaeoecology, v. 308, no. 1-2, p. 1-11.

Andersson, A., Kuffner, I., Mackenzie, F., Jokiel, P., Rodfers, K., and Tan, A., 2009, Net loss of $CaCO_3$ from a subtropical calcifying community due to seawater acidification: mesocosm-scale experimental evidence: Biogeosciences, v. 6, p. 1811-1823. Doi:10.5194/bg-6-1811-009.

Basu, A.R. Petaev, M.I., Poreda, R.J., Jacobsen, S.B., and Becker, L., 2003, Chondritic meteorite fragments associated with the Permian-Triassic boundary in Antarctica: Science, v. 302, p. 1388-1392. doi: 10.1126/science.1090852.

Baud, A., Cirilli, S., and Marcoux, J., 1997, Biotic response to mass extinction: the lowermost Triassic microbialites: Facies, v. 36, p. 238-242.

Baud, A., Richoz, S. Cirilli, S., and Marcoux, J., 2002, Basal Triassic carbonate of the Tethys: a microbialite world *in* 16th International Sedimentological Congress, Johannesburg, v. 8, p. 24-25.

Baud, A., Richoz, S., and Pruss, S., 2007, The lower Triassic anachronistic carbonate facies in space and time: Global Planetary Change, v. 55, no. 1-3, p. 81-89.

Becker, L., Poreda, R.J., Hunt, A.G., Bunch, T.E., and Rampino, M., 2001, Impact event at the Permian-Triassic boundary: Evidence from extraterrestrial noble gases in fullerenes: Science, v. 291, p. 1530-1533. dog:110.1126/science.1057243.

Benton, M.J., and Newell, A.J., 2014, Impacts of global warming on Permo-Triassic terrestrial ecosystems: Gondwana Research, v. 25, p. 1308–1337. doi.10.1016/j.gr.2012.12.010.

Bérczi-Makk, A., 1987, Earlandia (Foraminifera) species from the Permian-Triassic boundary in N Hungary: Magyar Állami Földtani Intézet evi Jelentése Az 1985, Évről, v. 1987, p. 215–226.

Black, B.A., Elkins-Tanton, L., Rowe, M.C., and Peate, I.U., 2012, Magnitude and consequences of volatile release from the Siberian Traps: Earth Planetary Science Letters, v. 317-318, p. 363-373.

Bottjer, D.J., Clapham, M.E., Fraiser, M.L., and Powers, C.M, 2008, Understanding mechanisms for the end-Permian mass extinction and the protracted Early Triassic aftermath and recovery: GSA Today, v. 18, p. 4–10.

Bowring, S.A., Erwin, D.H., Jin, Y.G., Martin, M.W., Davidek, K., and Wang W., 1998, U/Pb Zircon Geochronology and Tempo of the End-Permian Mass Extinction: Science, v. 280(5366), p. 1039-1045.

Briegleb, B.P., Bitz, C.M., Hunke, E.C., Lipscomb, W.H., Holland, M.M., Schramm, J.L., and Moritz, R.E., 2004: Scientific description of the sea ice component in the Community Climate System Model, Version Three, Tech Rep. NCAR/TN-463+STR, National Center for Atmospheric Research, Boulder, CO, 78 p.

Brand, U., Posenato, R., Came, R., Affek, H., Angiolini, L., Azmy, K., and Farabegoli, E., 2012, The end-Permian mass extinction: A rapid volcanic CO_2 and CH_4-climatic catastrophe: Chemical Geology, v. 322–323, p. 121– 144, https://doi.org/10.1016/j.chemgeo.2012.06.015.

Brönnimann, P., Zaninetti, L., and Bozorgnia, F., 1972, Triassic (Scythian) smaller foraminifera from the Elika formation of the central Alborz, northern Iran, and from the Siusi formation of the Dolomites, northern Italy: Mitteilungen Der Gessellschaft Der Geologie Und Bergbaustudenten, v. 21, p. 861–884.

Caldeira, K., and Kasting, J.F., 1992, The life span of the biosphere revisited: Nature, v. 360, no. 6406, p. 721-723.

Caldeira, K., and Wickett, M.E., Anthropogenic carbon and ocean pH: Science, v. 425, p. 365.

Chave, K.E., 1967, Recent carbonate sediments-an unconventional view: Journal of Geological Education, v. 15, no. 5, p. 200-204.

Charlson, R.J., Lovelock, J.E., Andreae, M.O., and Warren, S.G., 197, Oceanic phytoplankton, atmospheric sulphur, cloud albedo and climate: Nature, v. 326, p. 655-661.

Cohen, K.M., Finney, S.C., Gibbard, P.L., and Fan, J.X., 2013, The ICS International Chronostratigraphic Chart: Episodes, v. 36, no. 3, p. 199-204.

Computational and Information Systems Laboratory. 2019. Cheyenne: HPE/SGI ICE XA System (Wyoming-NCAR Alliance). Boulder, CO: National Center for Atmospheric Research. doi:10.5065/D6RX99HX.

Collins, W.D., Rasch, P.J., Boville, B.A., Hack, J.J., McCaa, J.R., Williamson, D.L., Kiehl, J.T., Briegleb, B.P., Bitz, C.M., Lin, S.J., and Zhang, M., and Dai, Y., 2004: Description of the NCAR community atmosphere model (CAM 3.0), Tech Rep. NCAR/TN-464+STR, National Center for Atmospheric Research, Boulder, CO, 214 p.

Collins, W.D., Rasch, P.J., Boville, B.A., Hack, J.J., McCaa, J.R., Williamson, D.L., Briegleb, B.P., Bitz, C.M., Lin, S.J., and Zhang, M., 2006a, The formulation and atmospheric simulation of the Community Atmosphere Model version 3 (CAM3): Journal of Climate, v. 19, no. 11, p. 2144-2161.

Collins, W.D., Bitz, C.M., Blackmon, M.L., Bonan, G.B., Bretherton, C.S., Carton, J.A., Chang, P., Doney, S.C., Hack, J.J., Henderson, T.B., Kiehl, J.T., Large, W.G., McKenna, D.S., Santer, B.D., and Smith, R.D., 2006, The Community Climate System Model Version 3 (CCSM3): Journal of Climate, v. 19, no.11, p. 2122-2143.

Dickinson, R.E., Henderson-Sellers, A., and Kennedy, J., 1993: Biosphere-atmosphere transfer scheme (BATS) version 1e as coupled to the NCAR community climate model, Tech Rep. NCAR/TN-387+STR, National Center for Atmospheric Research, Boulder, CO, p. 80. doi:10.5065/D67W6959

Doney, S.C., Fabry, V.J., Feely, R.A., and Kleypas, J.A., 2009, Ocean acidification: the other CO_2 problem: Annual Review of Marine Science, v., 1, p. 169-192.

Edwards, L.E., 1984, Insights on why graphic correlation (Shaw's method) works: The Journal of Geology, v. 92, p. 583-597. doi:10.1086/628893.

Edwards, L.E., 1989, Supplemented graphic correlation: A powerful tool for paleontologists and nonpaleontologists: Palaios, v. 4, p. 127-143. doi: 10.2307/3514601.

Ellwood, B.B., Wardlaw, B.R., Nestell, M.K., Nestell, G.P., Luu, T.P.L., 2017, Identifying globally synchronous Permian-Triassic boundary levels in successions in China and Vietnam using Graphic Correlation: Palaeogeography, Palaeoclimatology, Palaeoecology, v. 485, p. 561-571.

Erwin, D.H., 1994, The Permo-Triassic extinction: Nature, v. 367, p. 231-236.

Fagerstrom, J.A., 1987, The evolution of reef communities: New York, John Wiley & Sons, 600 p.

Fielding, C.R., Frank, T.D., Vajda, V., McLoughlin, S., Mays, C., Tevyaw, A.P., Winguth, A., Winguth, C., Nicoll, R.S., Bocking, M., and Crowley, J.L., 2019, Age and pattern of the southern high-latitude continental end-Permian extinction constrained by multiproxy analysis: Nature Communications, v. 10, no. 385. https://doi .org/10.1038/s41467-018-07934-z.

Foster, G.L., Royer, D.L., and Lunt, D.J., 2017, Future climate forcing potentially without precedent in the last 420 million years: Nature Communications, v. 8, p. 14845.

Fraser, R.H., and Currie, D.J., 1996, The species richness-energy hypothesis in a system where historical factors are thought to prevail: coral reefs: The American Naturalist, v. 148, no. 1, p.138-159.

Fu, Q., Johanson, C.M., Wallace, J.M., Riechler, T., 2006, Enhanced Mid-Latitude Tropospheric Warming in Satellite Measurements: Science, v. 312, no. 5777, p. 1179.

Gautam, M.D., 2018, Simulation of Climate Across the Permian-Triassic Boundary with a Focus on Phytogeographical Data Analysis [M.S. thesis]: Arlington, University of Texas, 51 p.

Gibbs, M.T., Rees, P.M., Kutzbach, J.E., Ziegler, A.M., Behling, P.J., and Rowley, D.B., 2002, Simulations of Permian climate and comparisons with lithological proxies: Journal of Geology, v. 110, p. 33-55.

Glynn, P.W., 1993, Coral reef bleaching: ecological perspectives: Coral reefs, v. 12, no. 1, p. 1-17.

Gordon, W.A., 1975, Distribution by Latitude of Phanerozoic Evaporite Deposits: The Journal of Geology, v. 83, no. 6, p. 671-684.

Groves, J.R., Altiner, D., and Rettori, R., 2005, Extinction, survival, and recovery of lagenide foraminifers in the Permian-Triassic boundary interval, Central Taurides, Turkey: Journal of Paleontology, v. 79, no. sp62, p. 1–38.

Groves, J.R., Rettori, R., Payne, J.L., Boyce, M.D., and Altiner, D., 2007, End-Permian mass extinction of lagenide foraminifers in the Southern Alps (northern Italy): Journal of Paleontology, v. 81, p. 415–434. doi:10.1666/05123.1

Gyllenhaal, E.D., Engberts, C.J., Markwick, P.J., Smith, L.H., and Patzkowsky, M.E., 1991, The Fujita-Ziegler model: a new semi-quantitative technique for estimating paleoclimate from paleogeographic maps: Paleogeography, Palaeoclimatology, Palaeoecology, v. 86, p. 41-66.

Hallam, A., 1985, A review of Mesozoic climates: Journal of the Geological Society, London, v. 142, p. 433-445.

Hallam, A., 1989, The case for sea-level changes as a dominant casual factor in mass extinction of marine invertebrates: Philosophical Transactions of the Royal Society of London B, v. 325, p. 437-455.

Hallam, A., 1991, Why was there a delayed radiation after the end-Paleozoic extinctions?: Historical Biology, v. 5, no. 2-4, p. 257-262.

Hallam, A., and Wignall, P.B., 1997, Mass extinctions and their aftermath: Oxford, Oxford University Press, p. 320.

Helby, R., 1973, Review of Late Permian and Triassic paly-nology of New South Wales: Geological Society of Australia Special Publication 4, p. 141–155.

Hudspith, V.A., Rimmer, S.M., and Belcher, C.M., 2014, Latest Permian chars may derive from wildfires, not coal combustion: Geology, v. 42, p. 879-882. doi: 10.1666/05123.1.

Isozaki, Y., 1997, Permo-Triassic boundary superanoxia and stratified superocean: records from lost deep sea: Science, v. 276, p. 235-238.

James, N.P., 1997, The cool-water carbonate deposition realm *in* James, N.P., Clarke, J., eds., Cool-water Carbonates: SEPM Society for Sedimentary Geology, Special Publication, Volume 56, p. 1-20.

Joachimski, M.M., Lai, X., Shen, S., Jiang, H., Luo, G., Chen, B., Chen, J., and Sun, Y., 2012, Climate warming in the latest Permian and the Permian-Triassic mass extinction: Geology, v. 40, p. 195-198. doi: 10.1130/G32707.1.

Kaiho, K., Kajiwara, Y., Nakano, T., Miura, Y., Kawahata, H., Tazaki, K., Ueshima, M., Chen, Z., and Shi, G.R., 2001, End-Permian catastrophe by a bolide impact: Evidence of a gigantic release of sulfur from the mantle: Geology, v. 29, p. 815-818. doi: 10.1130/0091-7613(2001)029<0815:EPCBAB>2.0CO;2

Kamo, S.L., Czamanske, G.K., Amelin, Y., Fedorenko, V.A., Davis, D.W., and Trofimov, V.R., 2003, Rapid eruption of Siberian flood-volcanic rocks and evidence for coincidence with the Permian-Triassic boundary and mass extinction at 251 Ma: Earth and Planetary Science Letters, v. 214, p. 75-91. doi:10.1016/S0012-821X(03)00347-9.

Kay, J.E., Hillman, B.R., Klein, S.A., Zhang, Y., Medeiros, B., Pincus, R., Gettelman, A., Eaton, B., Boyle, J., Marchand, R., and Ackerman, T.P., 2012, Exposing global cloud biasis in the Community Atmosphere Model (CAM) using satellite observations and their corresponding instrument simulators: Journal of Climate, v. 25, p. 5190-5207.

Kemple, W.G., Sadler, P.M., and Srauss, D.J., 1995, Extending graphic correlation to many dimensions: Stratigraphic correlation as constrained optimization, *in* Mann, K.O., and Lane, H.R., ed., Graphic correlation: Society of Economic Paleontologists and Mineralogists Special Publication, Volume 53, p. 65-82.

Kidder, D.L., and Worsley, T.R., 2004, Causes and consequences of extreme Permo-Triassic warming to globally equable climate and relation to the Permo-Triassic extinction and recovery: Palaeogeography, Palaeoclimatology, Palaeoecology, v. 203, p. 207-237.

Kidder, D.L., and Worsley, T.R., 2012, A human-induced hothouse climate: GSA Today, v. 22, p. 4-11.

Kiehl, J., and Shields, C.A., 2005, Climate simulation of the latest Permian: Implications for mass extinction: Geology, v. 33, p. 757-760.

Kiehl, J. and Shields, C.A., 2013, Sensitivity of the Palaeocene-Eocene Thermal Maximum climate to cloud properties: Philosophical Transactions of the Royal Society A Mathematical Physical and Engineering Sciences, 371:20130093.

Kiessling, W., and Simpson, C., 2011, On the potential for ocean acidification to be a general cause of ancient reef crises: Global Change Biology, v. 17, no. 1, p. 56-67.

King, G.M., 1991, Terrestrial tetrapods and the end-Permian event: a comparison of analyses, Historical Biology, v. 5, no. 2-4, p. 239-255.

Köppen, W., A. Wegener, 1924: Die Klimate der geol- ogischen Vorzeit (The climates of the geological past) Borntraeger, Berlin.

Korte, Ch., Pande, P., Kalia, P., Kozur, H.W., Joachimski, M.M., and Oberhänsli, H., 2010, Massive volcanism at the Permian-Triassic boundary and its impact on the isotope composition of the ocean and atmosphere: Journal of Asian Earth Sciences, v. 37, p. 293-311. doi: 10.1016/j.jseaes.2009.08.012.

Kozary, M.T., Dunlap, J.C., Humphrey, W.E., 1968, incidence of saline deposits in geologic time: Geological Society of America Special Paper 88, p. 43-57.

Kozur, 1996. The conodonts Hindeodus, Isarcicella and Sweetohindeodus in the uppermost Permian and lowermost Triassic: Geologica Croatica, v. 49, no. 1, p. 81-115.

Kroeker, K.J., Kordas, R.L., Crim, R., Hendricks, I.E., Ramajo, L., Singh, G.S., Duarte, C.M., and Gattuso, J.P., 2013, Impacts of ocean acidification on marine organisms: quantifying sensitivities and interaction with warming: Global Change Biology, v. 19, p. 1884-1896.

Kump, L.R., and Lovelock, J.E., 1995, The geophysiology of climate *in* Henderson-Sellers, A., eds., World Survey of Climatology: Amsterdam, Netherlands, Elsevier Science, Volume 16, p. 537-551.

Kump, L.R., Pollard, D., 2008, Amplification of Cretaceous warmth by biological cloud feedbacks: Science, v. 320, p. 195.

Kutzbach, J.E., Gallimore, R.G., 1989, Pangean climates: Megamonsoons of the megacontinent: Journal of Geophysical Research: Atmospheres, v. 94(D3), p. 3341-3358.

Lai, X.L., Wignall, P.B., Zhang, K.X., 1998, Paleoecology of conodont Hindeodus and Clarkina across the Permian-Triassic boundary: Geological Society of America Abstracts with Programs, A-310.

Laurie, J.R., Bodorkos, S., Nicoll, R.S., Crowley, J.L., Mantle, D.J., Mory, A.J., Wood, G.R., Backhouse, J., Holmes, E.K., Smith, T.E., and Champion, D.C., 2016, Calibrating the middle and Late Permian palynostratigraphy of Australia to the geologic time-scale via U–Pb zircon CA-ID-TIMS dating: Australian Journal of Earth Sciences, v. 63, p. 701–730, https://doi.org/10.1080/08120099.2016.1233456.

Lan, L.T.P., Ellwood, B.B., Tomkin, J.H., Nestell, G.P., Nestell, M.K., Ratcliff, K.T., Rowe, H., Huyen, D.T., Dung, N.T., Thang, N.C., Thanh, N.H., and Quyen D.V., 2018, Correlation and high-resolution for Paleo-tethys Permian-Triassic boundary exposures in Vietnam and Slovenia using geochemical, geophysical and biostratigraphic data sets: Vietnam Journal of Earth Sciences, v. 40, no. 3, p. 253-270.

Lehrmann, D.J., 1999, Early Triassic calcimicrobial mounds and biostromes of the Nanpanjiang Basin, South China: Geology, v. 27, p. 359-362.

Lehrmann, D.J., Wan, Y., Wei, J., Yu, Y., and Xiao, J., 2001, Lower Triassic peritidal cyclic limestone; an example of anachronistic carbonate facies from the Great Bank of Guizhou, Nanpanjiang Basin, Guizhou Province, South China: Palaeogeography, Palaeoclimatology, Palaeoecology, v. 173, p. 103-123.

Lehrmann, D.J., Payne, J.L., Felix, S.V., Dillet, P.M., Youyi, H.W., Yu, Y., and Wei, J., 2003, Permian-Triassic boundary sections from shallow marine carbonate platforms of the Nanpanjiang Basin, South China: Implications for oceanic conditions associated with the end-Permian mass extinction and its aftermath: Palaios, v. 18, p. 138-152.

Leonard, J.E., Cameron, B., Pilkey, O.H., and Friedman, G.M., 1981, Evaluation of cold-water carbonates as a possible paleoclimatic indicator: Sedimentary Geology, v. 28, no. 1, p. 1-28.

Lottes, A.L., and Ziegler, A.M., 1994, World peat occurrence and the seasonality of climate and vegetation *in* The Euramerican Coal Province: Controls on Tropical Peat Accumulation in Late Paleozoic: Palaeogeography, Palaeoclimatology, Palaeoecology, v. 106, p 23-37.

Lovelock, J.E., and Kump, L.R., 1994, Failure of climate regulation in a geophysical model: Nature, v. 369, p. 732-734.

Manabe, S., Wetherald, R., 1980, On the distribution of climate chance resulting from an increase in CO2 content of the atmosphere: Journal of Atmospheric Sciences, v. 37, no. 1, p. 99-118.

Manzello, D.P., Kleypas, J.A., Budd, D.A., Eakin, C.M., Glynn, P.W., and Langdon, C., 2008, Poorly cemented coral reefs of the eastern tropical Pacific: Possible insights into reef development in a high-CO2 world: Proceedings of the National Academy of Sciences, v. 105, no. 30, p. 10450-10455.

Martin, M.W., Lehrmann, D.J., Bowring, S.A., Enos, P., Ramezani, J., Wei, J., and Zhang, J., 2001, Timing of Lower Triassic carbonate bank buildup and biotic recovery following the end-Permian extinction across the Nanpanjiang Basin, South China: Geological Society of America Abstracts with Programs, v. 33, no. 6, p. 201.

Maxwell, W., 1992, Permian and early Triassic extinction of non-marine tetrapods: Paleontology, v. 35, p. 571-583.

Metcalfe, I., Crowley, J.L., Nicoll, R.S., and Schmitz, M., 2015, High-precision U-Pb CA-TIMS calibration of Middle Permian to Lower Triassic sequences, mass extinction and extreme climate-change in eastern Australian Gondwana: Gondwana Research, v. 28, p. 61-81.doi: 10.1016/j.gr.2014.09.002.

McElwain, J. C., Punyasena, and S.W., 2007, Mass extinction events and the plant fossil record: Trends in Ecology & Evolution, v. 22, no. 10, p. 548–557. doi:10.1016/j.tree.2007.09.003. PMID17919771

Michaelsen, P., 2002, Mass extinction of peat-forming plants and the effect on fluvial styles across the Permian–Triassic boundary, northern Bowen Basin, Australia: Palaeogeography, Palaeoclimatology, Palaeoecology, v. 179, p. 173–188. doi: 10.1016/S0031-0182(01)00413-8.

Müller, R. D., Cannon, J., Qin, X., Watson, R. J., Gurnis, M., Williams, S., Pfaffelmoser, T., Seton, M., Russell, S. H. J., and Zahirovic, S., 2018, GPlates: Building a virtual Earth through deep time: Geochemistry, Geophysics, Geosystems, v. 19. doi:10.1029/2018GC007584.

Mundil, R., Ludwing, K.R., Metcalfe, I., Renne, P.R., 2004, Age and timing of the Permian mass extinctions: U/Pb dating of closed-system zircons: Science, v. 305, p. 1760-1763.

Nestell, G.P., Nestell, M.K., Ellwood, B.B., Wardlaw, B.R., Basu, A.R., Ghosh, N., Luu, T.P.L, Rowe, H.D., Hunt, A., Tomkin, J.H., and Ratcliffe, K.T., 2015, High influx of carbon in walls of agglutinated foraminifers during the Permian-Triassic transition in global oceans: International Geology Review, v. 57, p. 411-427.

Oleson, K.W., Dai, Y., Bonan, G., Bosilovich, M., Dickinson, R., Dirmeyer, P., Hoffman, F., Houser, P., Levis, S., Niu, GY., Thornton, P., Vertenstein, M., Yang, ZL., Zeng, X., 2004: Technical description of the Community Land Model (CLM), Tech Rep. NCAR/TN-461+STR, National Center for Atmospheric Research, Boulder, CO, 174 p.

Orr, J.C., Fabry, V.J., Aumont, O., Bopp, L., Doney, S.C., Feely, R.A., Gnanadesikan, A., Gruber, N., Ishida, A., Joos, F., and Key, R.M., 2005, Anthropogenic ocean acidification over the twenty-first century and its impact on calcifying organisms: Nature, v. 437, no. 7059, p. 681-686.

Osen, A., 2014, Sensitivity of the Late Permian Climate to Tectonic and Radiative Forcing Changes: Implications for Mass Extinction [Ph.D. thesis]: Arlington, University of Texas, 153 p.

Parrish, J.T., Ziegler, A.M., Scotese, C.R., 1982: Palaeogeography, Palaeoclimatology, Palaeoecology, v. 40, p. 67-101.

Payne, J.L., Lehrmann, D.J., Wei, J., and Knoll, A.H., 2006, The Pattern   and Timing of Biotic Recovery from the End-Permian Extinction on the Great Bank of Guizhou, Guizhou Province, China: Palaios, v. 21, no. 1, p. 63-85.

Payne, J., Turchyn, A., Paytan, A., Depaolo, D., Lehrmann, D., Yu, M., and Wei, J., 2010, Calcium isotope constraints on the end-Permian mass extinction: Proceedings of the National Academy of Sciences of the United States of America, v. 107, no. 19, p. 8543–8548. doi:10.1073/pnas.0914065107.

Payne, J.L., and Clapham, M.E., 2012, End-Permian mass extinction in the oceans: An ancient analog for the twenty-first century?: Annual Review of Earth and Planetary Sciences, v. 40, no. 1, p. 89-111.

Pruss, S.B., and Bottjer, D.J., 2004, Early Triassic Trace Fossils of the Western United States and their Implications for prolonged Environmental Stress from the End-Permian Mass Extinction: Palaios, v. 19, no. 6, p. 551-564.

Pruss, S.B., and Bottjer, D.J., 2005, The reorganization of reef communities following the end-Permian mass extinction: Earth-science reviews, v. 78, no. 3-4, p. 193-206.

Raup, D.M., 1979, Size of the Permo-Triassic bottleneck and its evolutionary implications: Science, v. 206, p. 217-218. doi:10.1126/science.206.4415.217.

Rees, P.M., Ziegler, A.M., Gibbs, M.T., Kutzbach, J.E., Behling, P.J., and Rowley, D.B., 2002, Permian phytogeographic patterns and climates: new data and model comparisons: The Journal of Geology, v.110, p. 1-31.

Renne, P.R., and Basu, A.R., 1991, Rapid eruption of the Siberian traps flood basalts at the Permo-Triassic boundary: Science, v. 253, p. 176-179. doi: 10.1126/science.253.5016.176.

Renne, P.R., Black, M.T., Zichao, Z., Richards, M.A., and Basu, A.R., 1995, Synchrony and causal relations between Permian-Triassic boundary crisis and Siberian flood volcanism: Science, v. 269, p. 1413-1416. doi:10.1126/science.269.5229.1413.

Retallack, G.J., Sheldon, N.D., Carr, P.F., Fanning, M., Thompson, C.A., Williams, M.L., Jones, B.G., and Hutton, A., 2011, Multiple Early Triassic greenhouse crises impeded recovery from late Permian mass extinction: Palaeogeography, Palaeoclimatology, Palaeoecology, v. 308, p. 233-251.

Sabine, C.L., Feely, R.A., Gruber, B., Key, R.M., Le, K., Bullister, J.L., Wanninkhof, R., Wong, C.S., Wallace, D.W.R., Tilbrook, B., Millero, F.J., Peng, T.H., Kozyr, A., Ono, T., Rios, A.F., 2001, The Oceanic Sink for Anthropogenic CO2: Science, v. 305, p. 367.

Sadler, P.M., 2004, Quantitative biostratigraphy-Achieving finer resolution in global correlation: Annual Review of Earth and Planetary Sciences, v. 32, p. 187-213. doi: 10.1146/annurev.earth.32.101802.120428.

Schobben, M., Joachimski, M.M., Korn, D., Leda, L., Korte, C., 2014, Palaeotethys seawater temperature rise and intensified hydrological cycle following the end-Permian mass extinction: Gondwana Research, v. 26, p. 675-683.

Scotese, C.R., 1987, Plate tectonic development of the Circum-Pacific during the Early Paleozoic *in* Megard, F., Circum-Pacific Orogenic Belts and the Evolution of the Pacific Ocean Basin: American Geophysical Union, Geodynamics Series, v. 18, p. 49-57.

Scotese, C. R., 2001. Atlas of Earth History, Volume 1, Paleogeography, PALEOMAP Project, Arlington, Texas, 52 p.

Sellwood, B.W., Price, G.D., Shackleton, N.J., and Francis, J.E., 1993, Sedimentary facies as indicators of Mesozoic palaeoclimate [and discussion]: Philosophical Transactions of the Royal Society of London Series B-Biological Sciences, v. 341, p. 225-233.

Shaw, A.B., 1964, Time in stratigraphy: New York, McGraw-Hill, p. 365.

Shen, S.Z., Crowley, J.L., Wang, Y., Bowring, S.A., Erwin, D.H., Sadler, P.M., Can, C.Z., Rothman, D.H., Henderson, C.M., Ramezani, J., Zhang, H., Shen., Y., Wang, X.D., Wang, W., Mu, L., Li, W.Z., Tang, Y.G., Liu, X.L., Liu, L.J., Zeng, Y., Jiang, Y.F., and Jin, Y.G., 2011, Calibrating the end-Permian mass extinction: Science, v. 334, p. 1367-1372.

Sloan, L.C., and Pollard, D., 1998, Polar stratospheric clouds: A high latitude warming mechanism in an ancient greenhouse world: Geophysical Research Letters, v. 25, p. 3517-3520.

Smith, R., Kortas, S., and Meltz, B., 1995: Curvilinear coordinates for global ocean models. Tech. Rep. LA-UR-95-1146, Los Alamos National Laboratory.

Smith, R., and Gent, P., 2002: Reference manual for the Parallel Ocean Program (POP), ocean component of the Community Climate System Model (CCSM2.0 and 3.0). Tech Rep. LA-UR-02-2484, Los Alamos National Laboratory.

Sun, Y., Joachimiski, M.M., Wignall, P.B., Yan, C., Chen, Y., Jiang, H., Wang, L., and Lai, X., 2012, Lethally Hot Temperatures during the early Triassic greenhouse: Science, v. 338, p. 366-370.

Svensen H., Planke S., Malthe-Sørenssen A., Jamtveit, B., Mykleburst, R., Rasmussen, E.T., and Rey, S.S., 2004, Release of methane from a volcanic basin as a mechanism for initial Eocene global warming: Nature, v. 429, no. 669, p. 542-5.

Svensen, H., Planke, S., Plozov, A.G., Schmidbauer, N., Corfu, F., Podladchikov, Y.Y., and Jamtveit, B., 2009, Siberia gas venting and the end-Permian environmental crisis: Earth and Planetary Science Letters, v. 277, p. 490-500.

Tribollet, A., Godinot, C., Atkinson, M., and Langdon, C., 2009, Effects of elevated pCO_2 on dissolution of coral carbonates by microbial euendoliths: Global Biogeochemical Cycles, v. 23, no. 3.

Twitchett, R.J., 1999, Palaeoenvironments and faunal recovery after the end-Permian mass extinction: Palaeogeography, Palaeoclimatology, Palaeoecology, v. 154, no.1–2, p. 27-37.

Upchurch, G.R., Kiehl, J., Shields, C., Scherer, J., Scotese, C., 2015, Latitudinal temperature gradients and high-latitude temperatures during the latest Cretaceous: congruence of geologic data and climate models: Geology, v. 43, p. 683-686.

Vernon, J.E.N., 1995, Coral reefs-an overview *in* Zann, L.P., and Kailola, P., eds., The State of the Marine Environment Report for Australia Technical Annex: 1 The Marine Environment: Great Barrier Reef Marine Park Authority, p. 135-144.

Wignall, P.B., and Twitchett, R.J., 1996, Oceanic Anoxia and the End Permian Mass Extinction: Science, v. 272(5265), p. 1155-8.

Wignall, P.B., 2001, Large igneous provinces and mass extinctions: Earth-Science Reviews, v. 53, no. 1-2, p. 1-33.

Wignall, P.B., and Twitchett, R.J., 2002, Extent, duration, and nature of the Permian-Triassic superanoxic event *in* Koeberl, C., MacLeod, K.C., eds., Catastrophic Events and Mass Extinctions: Impacts and Beyond: Geological Society of America Special Paper, p. 395-414.

Winguth, A.M.E., Heinze, C., Kutzbach, J.E., Maier-Reiner, E., Mikolajewicz, U., Rowley, D.B., Rees, P.M., and Ziegler, A.M., 2002, Simulated warm polar currents during the Middle Permian: Paleoceanography, v. 17, no. 4, 1057.

Winguth, A.M.E., Shields, C.A., Winguth, C., 2015, Transition into a Hothouse World at the Permian-Triassic boundary-A model study: Palaeogeography, Palaeoclimatology, Palaeoecology, v. 440, p. 316-327.

Winton, M., 2006, Amplified Artic climate change: what does surface albedo feedback has to do with it?: Geophysical Research Letters, v. 33, no. 3., L03701. Doi:10.1029/2005GL025244.

Woodroffe, C.A., Robertson, A.I., and Alongi, D.M., 1992, Mangrove sediments and geomorphology, in Robertson, A.I., Alongi, D.M., Tropical mangrove ecosystems, Coastal and Estuarine Studies, v. 41, p. 7-41.

Yates, K.K., and Halley, R.B., 2006, $CO_3{}^2$-concentration and pCO_2 thresholds for calcification and dissolution on the Molokai reef flat, Hawaii: Biogeosciences, v. 3, p. 357-369. doi:10.5194/bg-3-357-2006.

Yeager, S.G., Shields, C.A., Large, W.G., and Hack, J.J., 2006, The low-resolution CCSM3: Journal of Climate, v. 19, p. 2545-2566.

Yin, H., Zhang, K., Tong, J., Yang, Z., and Wu, S., 2001, The global stratotype section and point (GSSP) of the Permian-Triassic boundary: Episodes, v. 24, p. 102-114.

Ziegler, P.A., 1982, Geological Atlas of Western and Central Europe: New, York, Shell Internationale Petroleum Maatschappij, Volume 2, 130 p.

Ziegler, A.M., Hulver, M.L., Lottes, A.L., and Schmachtenberg, W.F., 1984, Uniformitarianism and palaeoclimates: inferences from the distribution of carbonate rocks *in* Brenchley, P.J., ed., Fossils and Climate, p. 3-25.

Ziegler, A.M., 1990, Phytogeographic patterns and continental configurations during the Permian Period *in* McKerrow, W.S., and Scotese, C.R., ed., Palaeozoic Palaeogeography and Biogeography: Geological Society, London, Memoirs, Volume 38, p. 363.

Ziegler, A.M., Hulver, M.L., and Rowley, D.B., 1997, Permian world topography and climate *in* Martini, I.P., ed., Late glacial and postglacial environmental changes: Quarternary, Carboniferous-Permian and Proterozoic, p. 111-146.

Ziegler, A.M., Gibbs, M.T., and Hulver, M.L. 1998, A mini-atlas of oceanic water masses in the Permian period: Proceedings of the Royal Society of Victoria, v. 110, p. 323-343.

Ziegler, A., Eshel, G, Rees, P.M., Rothfus, T., Rowley, D., and Sunderlin, D., 2003, Tracing the tropics across land and sea: Permian to present: Lethaia, v. 36, no. 3, p. 227-254.

Biographical Information

Heather Nicole Brauer received a B.S. in Geology and an M.S. in Geosciences from the Department of Earth and Environmental Sciences from the University of Texas at Arlington. Her research in paleoclimate studies was guided by Dr. Arne Winguth and funded by the NSF grant EAR 1636629 and the College of Science. During her academic career she presented research at the Annual Celebration of Excellence by Students hosted by the College of Science and at conferences for the Geological Society of America. On campus she was actively involved in the Geological Society, Sigma Gamma Epsilon, and MavsGoGreen. After receiving her master's degree in December 2020, she intends to work in the industry.